Steviol Rebaudiosides bind to four different sites of the human sweet taste receptor (T1R2/T1R3) complex explaining confusing experiments

Shuang Hao[1], Brian Guthrie[2], Soo-Kyung Kim[3], Sergej Balanda[4], Jan Kubicek[4], Babar Murtaza[5], Naim A. Khan[5], Pouyan Khakbaz[2], Judith Su[1,*], William A. Goddard III[3,*]

[1]Wyant College of Optical Sciences, The University of Arizona, Tucson, AZ 85721, USA
[2]Global Core Research and Development Group, Cargill, Inc. 14800 28th Avenue N. Plymouth, MN 55447, USA
[3]Materials and Process Simulation Center (MSC), California Institute of Technology, Pasadena, California 91125, USA
[4]Cube-biotech, Creative Campus Monheim, Creative-Campus-Allee 12, 40789 Monheim, Germany
[5]Physiologie de la Nutrition and Toxicologie, UMR U866 Institut National de la Santé et de la Recherche Médicale, Université de Bourgogne-Franche Compté, Agro-Sup Dijon, France
*Corresponding authors: wag@caltech.edu; judy@optics.arizona.edu

ORCID: WAG (0000-0003-0097-5716), SKK (0000-0002-4498-5441), BDG (0000-0002-3508-4625), JS (0000-0002-1005-1755)

Abstract

Sucrose provide sweetness and energy when it binds to both the Venus fly trap domains (VFD) of heterodimeric sweet taste receptor (T1R2/T1R3),[1] while non-caloric sweeteners (Sucralose, Aspartame, Neotame, Saccharin, Acesulfame-K (Ace-K), Suosan, SC-45647, Fructose, and D-Tryptophan) bind only at the VFD of T1R2 (VFD2) to provide high-intensity sweetness.[2] Here, we address the binding mechanism of various steviol glycosides (Rebaudioside B (RebB), RebM, RebD, Rubusoside (Rubu), RebC), artificial sweeteners (Neohesperidin dihydrochalcone (NHDC), acesulfame K, S-819, Amiloride, and Perillartine), and negative allosteric modulator (Lactisole) at four distinct binding sites, VFD2, VFD3, transmembrane domain 2 (TMD2) and TMD3 by performing binding experiments and computational docking studies. Our docking results find multiple binding sites for the tested ligands including the radio labelled ligands, which provides an explanation of the mixed data of the radio-ligand binding experiments. We predict different preferred binding sites depending on ligand modifications of steviol glycosides. Thus, Rubu binds best at VFD3, while RebB binds best at TMD3, while the others prefer VFD2. We also observed G protein-coupled receptor (GPCR) allostery using the label free Frequency Locking Optical Whispering Evanescent Resonator (FLOWER) method. We show experimentally that the C20 carboxy terminus of the Gα protein can bind to the intracellular region of either TMD2 or TMD3, which can alter GPCR affinity to the high-affinity state for steviol glycosides. These studies provide a mechanistic understanding of the structure and function of this heterodimeric sweet taste receptor that can guide rational structure-based design of novel non-caloric sweeteners aimed at enabling lower sugar usage levels while retaining the sweet taste. This may provide the basis for novel therapeutic applications for treatment of obesity and related metabolic dysfunctions such as diabetes.

Keywords: sweet taste receptor, GPCR, Rebaudiosides, receptor ligand binding

INTRODUCTION

Humans can perceive at least five taste qualities, including sweet, umami, bitter, sour, and salty.[3] Among these tastes, sweet taste plays a vital role in determining food choices. Sweet-tasting foods signify the presence of high-calorie carbohydrates, which are essential for supplying energy to the body through the digestive process. Consequently, individuals tend to gravitate towards consuming sweet foods and beverages.[4] Excessive calorie intake from carbohydrates can lead to obesity, increasing the risk of type 2 diabetes, cardiovascular diseases, and even certain cancers.[5] In response to these health concerns, there has been a development of non-caloric sweeteners, such as saccharin, known for its combination of bitter and sweet tastes[6]. Other non-caloric sweeteners, despite their higher sweetness compared to sucrose, fail to replicate the authentic taste, diminishing people's inclination to consume food containing these substitutes. In the pursuit of developing non-caloric sweeteners that mimic the sensory experience of sucrose, understanding the activation of sweet taste receptors becomes crucial, starting from the binding and activation processes of sweet ligands.

The human sweet taste receptor functions as a heterodimer comprised of T1R2 and T1R3 subunits. The T1R subunits belongs to the class C family of G protein-coupled receptors (GPCRs), which also includes metabotropic glutamate receptors (mGluRs)[7], the calcium-sensing receptor (CaSR)[8], and the γ-aminobutyric acid receptor (GABAR)[9]. The T1R subunits exhibit structural characteristics typical of a GPCR, as depicted in Fig. 1. It is characterized by a large extracellular Venus Flytrap Domain (VFD) coupled to a short cysteine-rich domain (CRD) that links the VFD to a seven-helix transmembrane domain (TMD).[10]

Typically, artificial sweet ligands bind to VFD2 in the T1R2/T1R3 heterodimer sweet taste receptor[1,11–17]. The agonist induces a conformational change in VFD2-VFD3 subdomains, transitioning from an open-open to a closed-open conformation. This closed-open structure is believed to contribute to the active state of the T1R2/T1R3 heterodimer sweet receptor[14]. The activation of the T1R2/T1R3 sweet receptor leads to the activation of a heterotrimeric G protein complex, consisting of a Gα subunit and a Gβγ dimer, triggering the exchange of guanosine diphosphate (GDP) for guanosine triphosphate (GTP) on the Gα subunit, causing the dissociation of the Gα subunit. This, in turn, stimulates downstream signaling in the sweet taste pathway, leading to the activation of various intracellular second messengers such as cyclic adenosine monophosphate (cAMP), inositol trisphosphate (IP3), and calcium ions[18] that ultimately generate neural impulses to central sensory centers.

The T1R2/T1R3 sweet taste receptors present multiple binding sites for sweet ligands, enabling activation by agonists with diverse structures and potencies. A prominent site is located at the VFD2 domain, accommodating natural sugars like fructose[19] and sucrose[20], as well as artificial non-caloric sweeteners such as aspartame[13], neotame[16], and acesulfame K (Ace-K)[21,22]. VFD2 also accepts natural sweet proteins like monellin[23] and brazzin[12]. While VFD3 in the T1R3 receptor has fewer interactions, the natural sugar sucrose binds both on the VFD2 and VFD3[14,20]. The TMDs interact with allosteric modulators and sweet compounds. For instance, artificial sweeteners (P-4000, perillartine) and positive allosteric modulator (PAM) S819[20,24] bind to TMD2. Negative allosteric modulators (NAMs) inhibiting sweet taste like amiloride interact with TMD2[25,26], whereas lactisole and Gymnemic acid (GA) bind to TMD3[16,27,28]. The artificial sweeteners, NHDC and cyclamate, bind to TMD3, enhancing the sweet taste sensation[27]. Sweet proteins, including thaumatin[29] and brazzein[12], interact with the CRD in the T1R3 subunit. When considering non-protein sweet ligands, potential binding sites include VFD2, VFD3, and the extracellular regions

of TMD2 and TMD3. The extracellular VFD structure, with two lobes, provides multiple binding pockets within VFD2 and VFD3, facilitating interactions with sweet ligands. The schematic model of the T1R2/T1R3 heterodimer sweet receptor in Fig. 1 illustrates these binding sites[27,30].

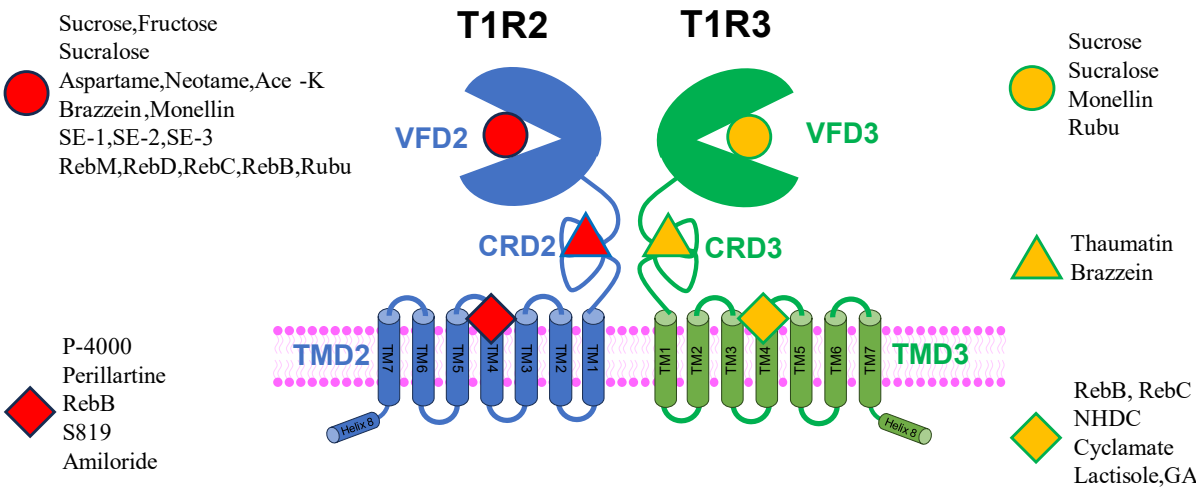

Figure 1. Schematic of human heterodimeric sweet taste receptor, T1R2/T1R3 and the binding sites preferred by various ligands.

Current research on the binding targets of the T1R2/T1R3 heterodimer, has characterized taste receptor agonists predominantly using heterologous cell-based assays that involve overexpressed GPCRs and promiscuous G proteins. These assays typically employ HEK 293 cells[24,31,32] or Flp-in 293[26–28,33] cells overexpressing the T1R2/T1R3 heterodimer and the Gα protein subunit. The concentration of calcium ion, a second messenger in the sweet taste downstream signaling pathway, is measured to assess the activation of the sweet taste receptor. To explore the specific functions of individual T1R subunits in the heterodimer sweet receptor, researchers can create cell lines expressing only one of the sweet receptor subunits. For example, HEK 293 cells expressing only human T1R2[21] and the human gastric cancer cell line HGT-1, where T1R3 is expressed via mRNA[34]. In contrast to heterologous clone expression in cell, the utilization of endogenous expression in natural cellular environments allows for a more physiologically relevant investigation into sweet taste receptor activation. In cultured mouse and human taste bud cells, agonists induce a swift increase in calcium levels by interacting with the lipid receptor GPR120[35,36]. Unlike the previous heterologous clone method, where cells are transduced with a virus encoding the promiscuous G protein, this approach employs dynamic mass redistribution (DMR) to measure stable clones overexpressing T1R2/T1R3 sweet taste receptors[37], allowing for effective coupling of the receptors to endogenous G proteins.

Sweetness perception, as a function of concentration, has long been related to the equilibrium binding affinity and binding kinetics[38,39]. Sweetener-receptor dissociation equilibrium constants (K_d) are the ratio of sweetener dissociation rate constant (k_{off}) and the association rate constant (k_{on}). The inverse of K_d, the K_a or association equilibrium constant, is called the affinity. Various models/ equations exist to account for multiple orthosteric binding sites, allosteric binding

behavior, constitutive activation, transducer/ efficacy models (R_{max}), agonist rebinding, blend synergies, and other receptor-ligand phenomenon[40–44].

Generally, in simpler models based on laws of mass action, the K_d has been one main marker for sweetener intensity since it is a measure of receptor occupancy which is needed for downstream signaling and signal amplification. Sweeteners usually show low affinities. So, generally, low affinity sweeteners need to have high concentrations to maintain high receptor activation. High concentrations could be limited by oral diffusion rates. Natural/ nutritive sweeteners have especially low affinities, making traditional binding studies difficult. High Intensity Sweeteners (HIS) sweeteners have higher affinities, but their maximum sweetness levels has been suspected to result from the ability to only bind at a subset of receptor locations available for nutritive sweeteners[45]. Ace-K and perillartine exhibit equilibrium constant values (K_d) values of 164 μM and 373 μM, respectively, in their interactions with human T1R2, as determined by the intrinsic fluorescence method.[21] Furthermore, circular dichroism (CD) measurements revealed a K_d of 100 μM for Ace-K when binding to the extracellular amino-terminal domain (ATD) of human T1R2.[46]

Experimentally, the Carboxy-terminus of the Gα protein, is in direct contact with the GPCR and dictates coupling specificity. Indeed the last 25 amino acid residues of GNAT3, function as the G protein coupled to the T1R2/T1R3 heterodimer sweet receptors[37]. The cell-based assay targeting sweet taste receptors evaluates responses indicative of sweet taste sensory signals, encompassing changes in calcium ion concentration and shifts in cellular mass distribution resulting from ligand binding. These sensory responses are quantified by determining the corresponding potency, expressed as the EC_{50}. RebA exhibits EC_{50} values of 57 μM in the DMR assay and 29 μM in the Fluorometric Imaging Plate Reader (FLIPR) assay,[37] showcasing consistency between the two techniques. In contrast, S-819 leads to a tenfold difference in potency, with an EC_{50} of 0.7 μM in the DMR assay and 0.07 μM in the FLIPR assay.[37] This observed variation might be influenced by the impact of the complex cellular environment on binding responses. Factors such as the Gα protein subunit, cAMP, and IP3 could exert an influence on downstream signaling in sweet taste, thereby affecting calcium release. For HEK293 cells stably expressing the human T1R2/T1R3 sweet taste receptor, reported EC_{50} values were 1.45 μM for Perillartine, 10.2 μM for NHDC, 14.4 μM for RebA, and 125 μM for Ace-K,[22] with RebM at 29.54 μM,[47] determined via FLIPR for calcium mobilization. Belloir et al. derived EC_{50} values of 2.54 μM for Perillartine and 213 μM for Ace-K using human T1R2/T1R3 heterodimers transiently transfected with a fluorescent calcium biosensor.[21] While the EC_{50} values for Ace-K align with its reported K_d of 100 μM,[46] Perillartine exhibited a substantial decrease compared to its reported K_d of 373 μM when T1R2 was expressed alone.[21] This inconsistency could be attributed to T1R2 potentially acting as a homodimer, diminishing binding affinity, or it could arise from variations in the cellular environment. Hence, we opted for a receptor-based assay to directly measure the binding response of the T1R2/T1R3 heterodimer, providing a more efficient representation of receptor binding responses and facilitating the investigation of agonist binding on the sweet taste receptor.

To investigate the agonist binding properties of sweet ligands on the T1R2/T1R3 receptors, the Isothermal Titration Calorimetry (ITC) method can be employed for measuring the thermodynamics of the molecular binding process[48]. Nuclear Magnetic Resonance (NMR) is utilized to identify and map sweet ligand and T1R2/T1R3 heterodimer receptor binding sites, employing Saturation Transfer Difference (STD) spectra[12]. The radioligand binding assay determines equilibrium dissociation constants for both radioligands and nonradioactive ligands,

providing insights into association and dissociation rates[49,50], albeit with limitations related to radio ligand depletion[51].

We apply the Frequency Locking Optical Whispering Evanescent Resonator (FLOWER) system to directly observe the response of sweet ligands binding to the receptor. This system utilizes a high-Q whispering gallery mode (WGM) microtoroid resonator highly sensitive to surrounding environmental disturbances[52–57]. The microtoroid's resonance shift serves as a signal representing the ligand binding response in T1R2/T1R3 sweet receptor assays, facilitated by the functionalization of the microtoroid surface with the sweet receptor.

Computationally based predictions of the 3D structures of GPCRs (GEnSeMBLE)[58,59] and of the binding sites for ligands (DarwinDock)[60] have played a major role in understanding the structures and functions of GPCRs. These calculations used "Complete Sampling" to examine 13 trillion rotations and tilts of the 7 TMD to select the best 25 for docking and examined ~50,000 docking sites to select first the best 100 and then the best case for building into the membrane. These methods have been validated for predictions of bitter taste receptors TAS2R[61–63] and for many class A GPCRs[64–72]. In particular, for Class A, we showed that the mechanism involves first precoupling of the inactive GPCR and the inactive GP (holding the GDP) to form a precoupled (partially activated) structure that opens to release GDP upon binding of agonist.[73] In contrast our earlier study of the T1R2/T1R3 sweet receptor (without the GP) concluded that binding of the agonist to VFD2 opens up the intracellular region of TMD3 to bind and activate the GP. For other class C cases it is not clear whether agonist binding or GP coupling is first, but we believe that GP coupling is first for the GABA receptor.[74] For Class B (GLP1[75]) and Class F (SMO[76]) more studies are needed to decide which is first. In this paper we consider binding of the ligands with and without the C25 terminal helix of Gα that plays an important role in activation.

A given sweet ligand may have several binding sites on the T1R2/T1R3 sweet receptor. For instance, sucrose, sucralose[1] and monellin[23,77] are reported to bind to both VFD2 and VFD3. The distinct sweetness of sucrose may be attributed to its multiple binding sites, which poses a challenge for creating non-caloric sweeteners that closely mimic sucrose's taste. Efforts are often made to formulate or develop sucrose-replaced non-caloric sweetness or sweetness blenders with low caloric content. Using the Temporal Check-All-That-Apply (TCATA) fading, it has been reported that blends of sucralose or erythritol with sucrose are suitable to mimic the sensory profile of sucrose[78]. The cyclamate/saccharin mixture demonstrates an intense sweetness, being 348 times sweeter than sucrose[79]. However, its sensory profile differs from sucrose and may not serve as an ideal substitute.

We have used Molecular dynamics (MD) provide hints on how sweeteners modulate the free energy landscape of the T1R2/T1R3 heterodimer[80]. Investigating the mechanism of synergy involves understanding the role of allosteric modulators in transmitting the sweet taste signal upon receptor activation. The novel PAMs: SE-1, SE-2, and SE-3, which bind to VFD2, have been identified to enhance the sucrose binding affinity without engaging in competition with agonists on VFD2.[17] However, their enhancement effect appears to be specific to certain responses of human sweet-taste receptors to neotame, sucrose, and sucralose.[32] In contrast, NHDC and cyclamate bind to TMD3, stimulating the sweet taste downstream signal and intensifying sweetness when interacting with various sweet compounds[22,27,81,82]. They have little impact on the binding affinity of the T1R2/T1R3 sweet heterodimer[83]. Notably, the NAM lactisole binds to a site that overlaps the binding pockets of cyclamate and NHDC on TMD3[81,84,85], acting as a broad antagonist that suppresses the sweet taste across different sweeteners[21,30,86]. Another NAM, GA,

shares the binding position on TMD3 with lactisole, inhibiting sweet taste responses to various sweetness[27]. However, GA's impact is more enduring due to its high binding affinity with TMD3, contrasting with lactisole rapid suppression effect upon removal[31]. Also, multiple binding could explain the potency limits of HIS where activation begins with a primary binding at a high affinity orthosteric site but is limited by a binding of the same ligand at a secondary low affinity negative allosteric site for "auto-antagonism". This effect could be confounded in most experimental binding studies.

To study the sensory mechanism of the sweet taste receptor, we start with activation of the T1R2/T1R3 heterodimer receptor. Based on the 3D predicted structure of the sweet receptor,[20] we employ MD simulations on direct and allosteric agonists to understand their impact on receptor conformation. Agonists bound to VFD2 induce significant conformational changes that progress from VFD2 through VFD3 to CRD3 and finally to TMD3, transforming the TMD dimer interface from the TM5/6 interface to the TM6 interface[20], which leads to G protein activation. While MD simulations provide support for G protein coupling to TMD3, the specific subunit to which the G protein couples remains ambiguous experimentally. Despite the understanding that the G protein must couple to the intracellular face of TMD in the heterodimer sweet receptor, the precise position—whether G protein couples to TMD2, TMD3, or both—remains undetermined. G protein coupling to each TMD region is a possibility. The TMD containing human T1R2 activates Gαi/o subunits[87]. Overexpression of human T1R2 in a HEK293S cell line has been shown to activate G proteins through perillartine binding to TMD2[21]. Concurrently, in HGT-1 cells expressing only T1R3 subunit receptors, sweet taste downstream signaling is induced by various sweet ligands[34].

In our investigation into the multiple binding sites of Steviol Rebaudiosides on human sweet taste receptors, a radioligand depletion experiment is used to explore the competitive binding dynamics among different sweet ligands. Analyzing the competitive binding results of Steviol Rebaudiosides against known binding site ligands proved instrumental in interpreting potential binding sites for Steviol Rebaudiosides. A critical parameter in our study was determining the binding constant K_d for Steviol Rebaudiosides. This investigation utilized the cell-free stable heterodimer method, enabling direct measurement of the binding response through monitoring the resonance shift of optical WGM resonator. Throughout the experiment, we meticulously controlled the presence or absence of G protein to assess the impact of G protein coupling to the TMD on the binding affinity of the T1R2/T1R3 heterodimer receptor. To complement our experimental findings, we employed computational docking mehtods to predict the preferred binding sites. This computational approach serves as a valuable reference for our experimental results and aids in predicting the binding affinity of different sites within the T1R2/T1R3 heterodimer. By prioritizing and optimizing experimental conditions, this integrated approach enhances our understanding of the binding characteristics of human sweet taste receptors.

METHODS

Two cell-free stable heterodimer methods were used including radioligand depletion with cloned sweet taste receptors and attached G proteins in a stable membrane preparation from taste bud cells, and frequency locked optical whispering evanescent resonator with attached stabilized heterodimer receptors cloned and expressed from heterologous cells and tested with a G protein 20-mer C-terminus peptide.

Receptor radioligand binding study: taste bud cell membrane assays

Various ligands were used based on their reported binding behavior: RebM (CAS 1220616-44-3) presumed binding at VFD2 , acesulfame-potassium (CAS 55589-62-3) reported binding at VFD2[12,14,16,17], RebC (CAS 63550-99-2) presumed binding at VFD2 , positive allosteric modifier S819 (CAS 902130-77-2, Thiourea, N-[4-(1-methylethoxy)phenyl]-N'-(1H-pyrrol-2-ylmethyl)-) reported binding at TMD2, amiloride HCL (CAS 2016-88-8) reported binding at TMD2[25], perillaratine (CAS 30950-27-7) reported binding at TMD2[25,32,32,82] and Neohesperidin dihydrochalcone (NHDC, CAS 20702-77-6) reported binding at TMD3[81].

The following radio-labelled ligands were selected for their binding at the different orthosteric and allosteric binding sites:

[^{3}H]-Lactisole: specific activity: 28.2 Ci/mmol (1.04 TBq/mmol), TMD3 binding site[85]

[^{3}H]-Perillartine: specific activity: 17.1 Ci/mmol (633 GBq/mmol), TMD2 binding site[82]

[^{3}H]-Rebaudioside B: specific activity: 3.2 Ci/mmol (85 GBq/mmol), presumed VFD2 binding site.

[^{14}C]-Sucrose: specific activity: 400-700 mCi/mmol (14.8 to 25.9 GBq/mmol), VFD2 and 3 binding site[1,88]

Sweeteners trigger a sweet taste by binding to lingual heterodimeric receptor (T1R2/T1R3). Most of the natural sugars like sucrose, glucose, and sucralose, bind to the extracellular domain, called VFD of T1R2 and T1R3, whereas dipeptide sweeteners, like aspartame and neotame, bind only to the T1R2 VFD. In the current study, we employed radioactive agents: [^{3}H]-Rebaudioside B, [^{3}H]-Perillartine and [^{3}H]-lactisole and assessed its binding to human taste bud cells. We also employed non-labeled ligands as competitors to calculate the binding kinetics.

Cell handling and isolation of cell membrane

Human taste bud cell lines were routinely grown and maintained in T75 flasks in IMDM medium supplemented with MCDB153 medium and serum. On the day of experimentation, cells were washed with PBS and scrapped off, followed by centrifugation at 1200 RPM for 5 minutes. The cell pellet was resuspended in ice-cold homogenization buffer (Tris HCl (pH 7.4) 20 mM, glycerol 10%, protease inhibitor cocktail) and homogenized by using Ultra Turrax homogenizer (24, 000 rpm). This was followed by centrifugation at 1500g for 15 min at 4°C to remove the cell debris and the resulting supernatant was centrifuged at 100 000 *g* for 60 min at 4°C to obtain cell membrane pellet which was re-suspended in homogenization buffer without protease inhibitors and kept at -80°C until use.

Saturation binding experiments

Saturation binding experiments were conducted in a total volume of 250 µL of homogenizing buffer per well (membrane 150 µL, cold ligand or buffer 50 µL, radioligand 50 µL). Incubation was done for 60 minutes at room temperature with gentle agitation and stopped by washing with filter harvester. The filter paper was cut and placed in scintillation counting tubes followed by the addition of scintillation liquid and radioactivity counting.

Kinetic binding experiments

Association assay (k_{on})

The incubation was started by adding 50 µL of radioligand. After 1, 2, 5, 10, 15, 20, 30, 45 and 60 minutes of incubation at room temperature, the 96 well plate was washed with water using filter-harvester, filter paper was appropriately cut and mixed with the scintillation liquid followed by scintillation counting, and analysis by GraphdPrism software using non-linear regression.

Dissociation assay (k_{off})

The dissociation assay was started after 1 hr of incubation with radioligand, by adding excess of cold ligand in a total assay volume of 250 µL. This time point at which dissociation was started was designated as the time zero. Afterwards, the 96-well plate was washed and scintillation was counted, as described earlier. Data were entered into GraphPad Prism software and k_{off}, k_{on} and k_d were determined using non-linear regression.

Competition binding experiments

Competition binding experiments were conducted by using fixed concentration of radioligand, and variable concentrations of unlabeled ligands. Radioligand and the competing agents were incubated for 1 hour, followed by washing and scintillation counting, as described previously. Concentrations were converted to log values and K_i (one site) was calculated by GraphPad Prism software using non-linear regression.

Effect of GTP and GDP on radioligand binding

It has been reported that the presence of GTP decreases agonist, but not antagonist binding in GPCRs[89]. Hence, radioligand displacement assays in the presence of increasing GTP and GDP concentrations were performed to evaluate the importance of the presence of a bound G protein. For this purpose, fixed concentrations of radioligands were used in the presence of increasing concentrations of GTP or GDP. IC_{50} values were calculated by using the GraphPad Prism software.

Stabilization of the human heterodimeric taste receptor T1R2/T1R3

A method was developed to generate human full-length heterodimeric taste receptor T1R2/T1R3 consisting of an expression screening, solubilization and stabilization screening and test purification for coupling the FLOWERS system for label free binding measurements.

Receptor constructs with different affinity tags are prepared and used for the transient expression in HEK293 cell culture. The literature for the heterodimeric receptor mainly describes experiments in which N-terminal affinity tags were used[90] for both, full-length or truncated protein versions[88]. Therefore, N-terminal tags are also used among others in this approach. Additionally, all expression constructs contain an Avi-tag for biotinylation and the wild-type signal peptide is exchanged to a HA signal sequence. As requested after expression a detergent and co-polymer screening as well as a test purification is performed. In contrast to detergents, DIBMAs and SMAs also isolate lipids from the cell wall contributing to membrane protein stabilization and have the capability to solubilize and form synthetic nanodisc in a single step. No further addition of DIBMA or SMA is needed during downstream processing.

Construct design and vector amplification

For expression and purification of human T1R2/T1R3 heterodimeric protein, both monomers were constructed on separate plasmids for co-expression. For T1R2, a HA signal peptide was added at

the N-terminus and a "GSSG" linker was added at the C-terminus followed by an Avi-tag and a FLAG tag. T1R3 was tagged with a N-terminal HA signal peptide and a C-terminal Avi-tag as well as a Rho1D4 tag separated from the protein sequence by "GSSG" linker. The protein sequences were constructed in a pcDNA3.4 vector backbone (Invitrogen). Both plasmids were amplified in E. coli TOP10 cells and purified with the endotoxin-free plasmid DNA purification system from Macherey-Nagel (NucleoBond® PC 10000 EF).

Co-expression of human T1R2 and T1R3 in Expi293F cells

The T1R2 and T1R3 plasmids were transiently co-transfected into Expi293F cells (Gibco) using polyethylenimine (PolySciences) at 2.5x106 cells/mL in Expi293 expression medium (Gibco) with 10 mM sucrose. The co-transfection was performed with a final DNA concentration of 1.5 µg/mL and 9 µg/mL PEI according to the manufacturer's instructions. The transfected cultures were incubated at 37°C with 6% CO2 and shaken at 110 rpm. After 20 hours, sodium butyrate and valproic acid were added with a final concentration of 10 mM and 5 mM, respectively. After 72 hours post transfection, the cells were collected by centrifugation (2,000x rpm; 15 min; 4° C) and supplemented with protease inhibitors: 10 µM Leupeptin, 1 mM o-Phenanthroline, 0.1 mM phenylmethylsulfonyl fluoride (PMSF); 10 µM E-64 (N-[N-(L-3-trans-Carboxyoxiran-2-carbonyl)-leucyl]-agmatin, N-(trans-epoxysuccinyl)-L-leucin-4-guanidinbutylamid) and 1 mM Pepstatin A in buffer containing 20 mM Hepes, 100 mM NaCl and 2 mM EDTA. Cell pellets were stored at -80°C until further use.

Purification and stabilization of human heterodimeric taste receptor T1R2/T1R3 in a synthetic nanodisc using DIBMA Glycerol

Frozen cells were resuspended in protein buffer (20 mM Hepes pH 8.0, 100 mM NaCl, 1 mM EDTA) supplemented with 10 µM Leupeptin, 1 mM o-Phenanthroline, 0.1 mM PMSF, 10 µM E-64 and 1 mM Pepstatin A. After sonication, cell debris were separated from membranes by centrifugation (9,000x g; 30 min; 4° C). The membranes were further pelleted by centrifugation (100,000x g; 1 h; 4 °C), and solubilized in protein buffer containing 2.5 % (w/v) DIBMA Glycerol (Cube Biotech GmbH, Monheim, Germany) overnight at 4 °C. Solubilized T1R2/T1R3 was separated from un-solubilized material by centrifugation (100,000× g; 1 h; 4 ◦C). The supernatant containing the target protein was diluted 1:10 with protein buffer and subsequently loaded onto a pre-equilibrated batch of Rho1D4-MagBeads (Cube Biotech GmbH, Monheim, Germany). To improve the binding, the MagBeads were incubated over night at 4 °C while gently stirring. Washing steps were performed with protein buffer five times under magnetic separation to remove non-specifically bound proteins. T1R2/T1R3 was eluted five time by incubating the beads with protein buffer containing 1 mg/mL Rho1D4 peptide for 30 min at 4°C. Elution samples were concentrated at 3,000x g (Amicon Ultra-15, Merck Millipore) and further analyzed by size exclusion chromatography on a Superose 6 increase column (GE Healthcare). Fractions corresponding to the heterodimeric size of T1R2/T1R3 were collected and concentrated. The protein concentration was determined with spectroscopic measurement at a wavelength of 280 nm and the quality was validated by SDS-PAGE and Western Blot using both, and Flag antibodies, separately. Protein samples were flash frozen and stored at −80 ◦C.

Gα C-terminal 20mer

The unmodified peptide sequence, VFDAVTDIIIKENLKDCGLF, of the GNAT3 C-terminal tail was synthesized for use in binding studies (Thermo Scientific Peptide Synthesis Service) at >98% purity.

Coupling of the Sweet Heterodimer to FLOWER

Microtoroid fabrication. Microtoroids are fabricated as previously described[91]. The microtoroid resonators are fabricated on silicon wafers with a 2 μm layer of thermally grown silica. First, circular disc patterns of photoresist with a diameter of 150 μm are patterned via photolithography on the top silica layer of the silicon wafer. These photoresist circular pads act as etch masks during immersion in buffered oxide etchant (BOE) solution (1:6 V/V) at room temperature. After wet etching, any residual photoresist and contaminants are removed using acetone and IPA (isopropyl alcohol). The wafer is then post-baked at 130°C to remove moisture. The remaining silica disks act as etch masks during exposure to xenon difluoride (XeF2) gas, resulting in uniform undercutting of the silica disks and the formation of silicon pillars that support the silica disks. A thermal reflow process using a CO_2 laser is used to shape the silica disk into a microtoroid.

Coupling of the sweet heterodimer to the microtoroid. The sweet heterodimer is coupled to the toroid via EDC/NHS coupling of an antibody amine. The toroid chip is first cleaned with ethanol then dried with nitrogen. The cleaned toroid chip is incubated in 1% v/v APTES in chloroform for 10 minutes to introduce amino groups onto the chip's surface. After incubation, the chip was thoroughly rinsed with chloroform to remove any excess APTES and dried with nitrogen. The chip was then incubated overnight in a succinic anhydride solution (100 mg of succinc anhydride in 1 mL of DMSO). The next day, the chip was rinsed sequentially with DMSO and ethanol to remove unreacted succinic anhydride and then blown dry.

For EDC/NHS antibody conjugation, EDC and NHS is equilibrated at room temperature for at least 30 minutes (1 hour recommended) before weighing. NHS and EDC are dissolved in 100 mM MES buffer to form a 100 mM EDC and 100 mM NHS mixed solution. An anti-FLAG (or anti-Rho) antibody solution is added to the mixed NHS/EDC solution to achieve a 30 nM concentration. The microtoroid is incubated in this solution for 15 minutes to ensure coupling. Following this activation step, the microtoroid chip is thoroughly rinsed with 100 mM MES buffer to remove any unreacted EDC/NHS and create a stable environment for subsequent functionalization.

Prior to microtoroid functionalization with the sweet heterodimer nanodiscs, the toroid chip is incubated in 100 mM ethanolamine for 5 minutes to block unreacted binding sites. The sweet heterodimer T1R2/T1R3 solution is diluted to 30 nM in HEN buffer. The chip is then incubated in the diluted T1R2/T1R3 heterodimer solution for 1 hour to ensure efficient coupling of the sweet heterodimer to the functionalized chip surface. After incubation, the toroid chip is rinsed thoroughly with HEN buffer. The functionalized microtoroid chip is then carefully transferred into an Eppendorf tube containing HEN buffer.

For T1R2/T1R3 sweet heterodimer coupling to the microtoroid, anti-FLAG will couple to the microtoroid. This coupling ensures that the sweet heterodimer (T1R2/T1R3) connects to the microtoroid through the TMD2 region, leaving the TMD3 region open for binding. In the experiments where it is desired to have the TMD2 region of the sweet heterodimer T1R2/T1R3 open, anti-FLAG can be replaced with anti-rho.

Binding measurements using FLOWER

We previously developed a system called Frequency Locked Optical Whispering Evanescent Resonator (FLOWER), which enables the rapid detection of single macromolecules in solution[53,91,92] as well as proteins[93,94] and exosomes[95] in complex solutions. FLOWER tracks resonance shifts resulting from the binding of molecules or nanoparticles to a WGM optical

resonator. WGM resonators are highly sensitive sensors[96] due to their long storage confinement times. They have a larger capture area than traditional plasmonic sensors[97], thus enabling rapid detection.[92] Unlike conventional methods that involve scanning the wavelength of a tunable probe laser, which can be limited by scanning speed and hinder real-time tracking of resonance shifts, FLOWER using frequency locking to reduce the response time and enhance the accuracy of resonance shift measurements. The experimental setup, as illustrated in Fig. S1, involves coupling a probe laser (PL) with a wavelength of 780 nm into a microtoroid resonator through a tapered optical fiber. To optimize the coupling efficiency between the tapered fiber and microtoroid, we control the polarization of the probe laser using a polarization controller (PC). A 2 kHz oscillation dither signal (DS) is input to the frequency modulation port of the probe laser for frequency modulation of the probe laser. The frequency modulated probe laser is split into two arms through a fiber-coupled beam splitter (BS). One arm carries the signal light coupled into the microtoroid through a tapered fiber, while the other serves as the reference light. Both the signal and reference light are then received by an auto-balanced receiver, which can reduce laser intensity noise by 55 – 70 dB.[98] By multiplying the auto-balanced receiver's electrical output signal by the DS and time-averaging, we obtain an error signal that is directly proportional to the wavelength detuning between the probe laser and the WGM resonance of the microtoroid. The error signal is zero when the probe laser precisely matches the microcavity resonance. Utilizing this error signal in a feedback loop to tune the laser through the frequency modulation port, the proportional-integral-derivative (PID) controller minimizes the error signal, thereby ensuring accurate and stable frequency locking of the probe laser to the microtoroid's resonance.

We record the resonance shift signal using a high-precision data acquisition card (NI PCI-4461) throughout sweet ligand binding experiments. Our toroidal optical microcavities are first functionalized with human T1R2/T1R3 heterodimer sweet taste receptors. In a pressure-driven prefusion system, we preload both the buffer and sweet ligand sample solution into multiple channels, allowing precise control over solution injection into the microfluidic chamber (Fig. S1) via a LabVIEW program. Initially, the microtoroid chamber undergoes flushing with HEN buffer, resulting in an initial red shift (shift to longer wavelengths) in resonance due to the self-heating of the microtoroid resonator caused by the circulating probe laser light. As we continuously inject HEN buffer, the resonance ceases to exhibit a red shift and stabilizes at a consistent value. This stabilization indicates that the microtoroid has achieved thermal equilibrium. Following this, we record the resonance shift signal curve to establish the sensor's baseline. We prepare a range of sweet ligand concentrations using the HEN buffer and sequentially inject them into the microfluidic chamber, starting from low concentrations and progressing to higher ones. Between each concentration, we rinse with running buffer, and measure the real-time resonance shift corresponding to each concentration. In the G protein C20 experiments, the HEN buffer is replaced by 10 μM C20 in HEN buffer. During injection, 10 μM C20 in HEN buffer is first introduced into the microfluidic chamber, and all sweet ligand solutions are supplemented with 10 μM C 20 to ensure that all ligands are under G protein C20 binding conditions.

In silico ligand binding energies

Predicting ligand binding sites without C20: Our studies used the full T1R2/T1R3 heterodimer structure predicted using GEnSeMBLE[58,59] for the TMD helixes. Our original initial structure used homology modeling for the VFD and CRD.[20] The detailed information is described in our previous paper.[20] For each ligand (Lactisole, NHDC, Ace-K, S-819, Amiloride, and Perillartine), we considered 10-15 torsional conformations in DarwinDock,[64] which iteratively generates ~50,000

poses in the putative binding regions for each of the 10-15 ligand conformations and each of the 25 GCPR configurations. The amino acid sidechains in the binding site were optimized for each of the best 100 ligand poses.[24] For each ligand conformation, the procedure was as follows. Starting from the minimized structure, we performed conformational searches of Mixed torsional/ Low-mode sampling (1000 steps, 1000 steps per rotatable bond, 10 kcal/mol energy window, 0.5 Å RMSD) using the Maestro software.[99] The low energy conformations were re-minimized using the Dreiding force field[20] with some modifications in the HB interactions and clustered by 2.0 and 1.0 Å of RMSD in two steps. For docking, low energy conformations for ligands from several clusters were selected. All ligand binding poses for Reb1-5, RebM, RebD, isoRebM, RebA, RebB, Rubu, RebC, and hydroxyRebM at VFD2 were used from the previous docking study.[20] For the binding poses at VFD3, TMD2 and TMD3, the additional sugars were extended from the best binding pose of Rubu from the docking study. To relax the binding site of the additional sugars, 10 cycles of annealing with the geometry constraint on the structure of Rubu were performed. After selecting the best energy conformer, another 1 cycle of annealing and full minimization using the Dreiding force field[20] was performed without constraints.

Generation of the C20 bound structure of T1R2/T1R3 heterodimer at TMD2 or TMD3: The various initial position of GNAT3 C20 were considered using the experimental structures of GPCR- G protein complexes, Class C mGlu2R-Gi (PDB ID: 7MTS[100], 7E9G[101]), mGlu4R-Gi (PDB ID: 7E9H[101]), GABAB2R-Gi (PDB ID: 7EB2)[102], and Class A OPRM-Gi (PDB ID 6DDF)[103]. We also included our predicted structure of the GNAT3-T1R2/T1R3 heterodimer complex.[104] After alignment of the GPCR backbone, all residues except the C-terminal 20 amino acids of the Gα protein were deleted followed by minimization of the fixed GPCR after the side chain refinement.

Full solvent MD: The C20 bound structure of the T1R2/T1R3 heterodimer at TMD2 or TMD3 were inserted into a continuous infinite POPC lipid bilayer membrane with periodic boundary conditions, while including full solvation with water at physiological salt concentration (0.9% concentration of NaCl, 154mM).

The disulfide bridges in TAS1R2 were constrained: C59-C102, C359-C363, C405-C410 in the VFD, C495-C514, C499-C517, C520-C535, C538-C551 in CRD, C233-C513 between VFD and CRD, and C630$^{3.25}$-C720 between TMD and EC2. The disulfide bridges in TAS1R3 were also constrained: C62-C103, C351-C370, C373-C375, C410-C415 in VFD, C499-C518, C503-C521, C524-C538, C541-C554 in CRD, C236-C517 between VFD and CRD, and C633$^{3.25}$and C722 between TMD and EC2.

The POPC lipid available in VMD was used to insert the protein into a lipid-water box, where lipids within 1 Å of the protein and waters within 2 Å of the protein were removed.

For the particle mesh Ewald (PME) in the electrostatics calculation,[105] the charge of system was balanced through replacing waters with Na^+ and Cl^- ions. After inserting the 7-helix bundle including loops into the box containing the periodic POPC membrane, water, and ions, we fixed the protein and minimized the lipid, water, ion atoms for 1,000 steps. We then equilibrated with NPT dynamics for 500 ps while continuing to keep the protein fixed. This allows the lipid and water to readjust to the protein. Then we minimized the full system for 1,000 steps and then performed NPT dynamics. This predicted structure was then equilibrated at 310 K using the NAMD 2.9 (NAnoscale Molecular Dynamics) program.[106] We used the CHARMM36 force field

parameters for the protein, the TIP3 model for water,[107] and the CHARMM27 force field parameters for the lipids.[108]

Predicting ligand binding sites at the C20 bound structure of T1R2/T1R3 heterodimer at TMD2 or TMD3: For the binding site of Rubu at the C20 bound structure of T1R2/T1R3 heterodimer at TMD2 or TMD3, the last trajectory of the C20 bound structure of T1R2/T1R3 heterodimer was aligned to the protein backbone of the binding site of Rubu at each domain (VFD2, VFD3, TMD2, and TMD3) from the previous docking study.[20] Then the matched complexes were annealed for 10 cycles between 50 to 600K. After an additional minimization, the lowest energy conformer was selected. For the binding site of RebM, RebD, and RebC, the additional sugars were extended from the best binding pose of Rubu. To relax the binding site of the additional sugars, we performed 10 cycles of annealing with geometry constraints on the structure of Rubu. After selecting the best energy conformer, another 1 cycle of annealing and full minimization using the Dreiding force field[20] were performed without any constraints.

In silico binding site discovery

The discovery of potentially undisclosed binding sites utilized a multi-step workflow. The apo-structure of the full hetero-dimer was used. SiteMap (Schrodinger)[109] was used to search for the ten best sites. Glide grids were made for each site then Glide[110,111] docking was performed to determine docking scores for the ligands. Molecular mechanics with generalised Born and surface area solvation (MM/GBSA) energies methods were run using Prime v[112] to determine binding site energies for potential new binding sites.

RESULTS

Radioligand binding studies: taste cell membrane assays

Kinetics of [^{3}H]-Rebaudioside B binding in the presence or absence of Ligands:

The Fig. S4 shows the results of kinetic binding experiments using [^{3}H]-Rebaudioside B as radioligand presumably bound at VFD2. Association was followed by dissociation which was initiated by adding excess (1000-fold) of cold Rebaudioside B at 60 min (time 0) after the start of incubation. [^{3}H]-Rebaudioside showed a k_{on} = 91.82 $M^{-1}min^{-1}$, k_{off} = 0.5321 min^{-1} and K_d = 0.005795 M. Addition of both GDP and GTP resulted in inhibition of Rebaudioside B binding. GDP had an IC_{50}= 2.152 mM (Fig. S5) while GTP had an IC_{50}= 9.222 mM (Fig. S6).

Competition binding experiments with various ligands with [^{3}H]-Rebaudioside B:

RebM showed ambiguous binding inhibition with RebB while RebC showed low competitive inhibition (Table S1). This was not expected since all the rebaudiosides are presumed to bind in the same VFD2 site. This could indicate that the RebC inhibition is generated at a binding site outside of the VFD2 site. The Ace-K and S819 results were expected. Ace-K was inhibited by RebB, presumably at the VFD2 site. S819 did not show strong inhibition with RebB and it has not been reported as binding in VFD2.

The positive inhibition results for NHDC and amiloride indicate that RebB may have the ability to bind in both TMD regions.

Kinetics of [^{3}H]-Lactisole binding in the presence or absence of ligands:

Association was followed by dissociation which was initiated by adding excess (1000-fold) of cold lactisole at 60 min (time 0) after the start of incubation. Lactisole was presumably bound on TMD3. [^{3}H]-Lactisole binding studies showed k_{on} = 217.7 $M^{-1}min^{-1}$, k_{off} = 0.01456 min^{-1} and K_d = 0.0000669 M (Fig. S7). No inhibition was seen with GDP (Fig. S8) or GTP (Fig. S9). Both GDP and GTP may induce an increase in lactisole binding.

Competition binding experiments using [^{3}H]-lactisole as radioligand:

Expected results were seen for NHDC (inhibition), Ace-K and S819. NHDC is known to bind TMD3 like lactisole while Ace-K and S819 do not. The positive inhibition seen with RebM and RebC was unexpected. This could indicate that either lactisole binds at other sites, such as the VFD2 or that RebC and RebM also bind at the TMD3 and are inhibited by lactisole. Since the lactisole site is known to be a negative allosteric binding site, the binding of these Rebs at this location could explain the low potency of these sweeteners where they bind at the TMD3 at high concentrations for a negative allosteric effect after the activation of the receptor by orthosteric binding at the VFD2 at lower concentrations. Relative binding energies are needed to determine if this is possible.

Kinetics of [^{3}H]-Perrilartine binding in the presence or absence of Cargill agents:

Association was followed by dissociation which was initiated by adding excess of cold Perillartine at 60 min (time 0) after the start of incubation. Perillartine presumably binds on TMD2. [^{3}H]-Perrilartine had a k_{on} = 184288 M-1min-1, k_{off} = 0.5337 min-1 and a K_d = 0.000002896 M (2.896 µM) (Fig. S10). Both GDP and GTP had an inhibitory effect on the binding of perillaratine (GDP IC_{50}= 12.65 mM, Fig. S11; GTP IC_{50}= 13.167 mM, Fig. S12).

Competition binding experiments using [^{3}H]-Perillartine as radioligand:

RebM and RebC showed on competitive inhibition with perillartine as expected since there are no reports of these binding in TMD2. However, amiloride and S819 are known to bind at TMD2 but did not show inhibition with perillartine. This was unexpected. Also unexpected were the high levels of inhibition seen with Ace-K and NHDC which are not known to bind at TMD2 and thus should not show such inhibition. The inhibition of NHDC could indicate that either NHDC can bind at TMD2 or that perillartine can bind at the TMD3 site where NHDC also binds.

Kinetics of [^{14}C]-sucrose binding in the presence or absence of ligands:

Radio-labeled sucrose binding was performed as mentioned above. This was to observe the target sweetener. Association was followed by dissociation which was initiated by adding excess of cold sucrose at 60 min after the start of incubation. [^{14}C]-sucrose showed k_{on} = 15.06 $M^{-1}min^{-1}$, k_{off} = 0.1863 min^{-1} and K_d = 0.0123 M (Fig. 13). This was expectedly higher than the previously mentioned high intensity sweeteners.

Competition binding experiments using [^{14}C]-sucrose as radioligand against NHDC:

As a method check, the binding competition between sucrose, a VFD2 and 3 binder and NHDC, a TMD3 binder, was performed. Inhibition was observed (K_i = 0.01362 M, Fig. S14).

During this study, very high K_d values have been observed that were in the millimolar range. These values were calculated from the kinetic binding experiments from the ratio of k_{off}/k_{on}. One earlier report has investigated the binding of sweet molecules to bovine taste bud cells.[113] K_d values

reported were of the order of millimolar, which corroborates our findings. For instance, the K_d value for sucrose was 1.1 mM and 3.4 mM for glucose. Such high K_d values may drastically affect the stability of radioligand-receptor complex during washings to separate bound from free ligand. While these dissociation constants and those observed during our study are significantly higher than the usually observed, they might represent a system with different physiological requirements. In taste system, loose binding may be of advantage as a tight binding will result in persistent taste sensation due to the stability of taste receptor-ligand complex and cause taste confusions. A weak taste receptor-tastant complex will subsequently allow the processing of new incoming taste information.

It is known that the presence of nucleotides decrease the binding of agonists but not antagonists with receptors[89]. We observed during the current study that binding of radioligands, i.e., [^{3}H]-Perillartine and [^{3}H]-RebB, decreased with increasing concentrations of GTP and GDP but not for [^{3}H]-Lactisole. This observation is consistent with the known agonist and antagonist activity of these molecules and indicates that the binding of these molecules depends on the availability of receptors that are coupled to a G protein[114]. Future studies should use labeled [^{35}S]-GTPγS could give a better understanding of the efficacy and effect on the binding of ligands and provide information about the possible allosteric modulation by other ligands[114].

FLOWER Binding Studies

Binding with and without C-20:

Upon binding to the T1R2/T1R3 receptor in FLOWER experiment, sweet ligands induce a red shift in the microtoroid's resonance. This shift arises from the interaction between receptor-ligand binding and the microtoroid's evanescent electrical field. Fig. S2 shows the binding response of Rubu and RebM. The binding response curve consistently exhibits a peak at approximately 150 seconds after sweet ligand injection, followed by a decrease and stabilization within the subsequent 400 seconds to a sustained response, representing around two-thirds to zero of the peak response magnitude. With increasing concentration, both the final stabilized binding response and peak value also increase. Previous work on DMR assays for the human sweet taste receptor has revealed that measuring the peak DMR response offers a more robust assay window compared to measuring the final and sustained DMR response[115].

Hence, we choose the peak response in the FLOWER resonance shift signal as the binding response in our human sweet taste receptor assays.

Binding curves were constructed by plotting the extracted resonance shift peak value as a function of ligand concentration. To determine the binding affinity, we employed a one-site specific binding model[116] that takes into account the background response and non-specific binding. The model is fit to the experimental data to assess the binding affinity and the Hill slope. The binding constant K_d and Hill slope n_H re determined through the curve fitting process according to the following equation:

$$\Delta\lambda = \frac{B_{max} * [L]^{n_H}}{{K_d}^{n_H} + [L]^{n_H}} + \mathrm{NS} * [\mathrm{L}] + B_{background},$$

where B_{max} is the maximum specific binding, $\Delta\lambda$ is the resonance shift at response peak, NS is the non-specific binding parameter, [L] represents the concentration of the sweet ligand solution, and $B_{background}$ is the background response. To create a normalized binding curve, we eliminated the background signal and non-specific binding response from the experimental data. Following this,

the data points were normalized by dividing each point by the maximum observed resonance shift in the dataset,

$$\Delta\lambda_{norm} = \frac{\Delta\lambda - B_{background}}{B_{max}} - \frac{\mathrm{NS} * [\mathrm{L}]}{B_{max}} = \frac{[L]^{n_H}}{{K_d}^{n_H} + [L]^{n_H}}$$

This normalization process enhances the clarity of the specific binding response curve, facilitating a more precise evaluation of the binding constant K_d and Hill slope n_H. The normalized binding curve and experiment data point are indicated in Fig. S3. The binding constant K_d is listed in Table 1 and the Hill slope n_H is listed in Table 2.

Table 1. Summary of binding constant K_d for T1R2/T1R3 with various sweet ligands

T1R2/T1R3	**RebC**	**Rubusoside**	**RebM**	**RebD**
TMD2 open (No C20)	342.6 μM	2.43 μM	185.9 nM	
TMD3 open (No C20)	84.42 μM	3.00 μM	21.92 nM	2.756 nM
TMD2 open (+C20)	0.592 μM		0.2797 nM	
TMD3 open (+C20)	1.085 μM	26.27 nM	2.56 nM	45.92 pM

Table 2. Summary of Hill slope n_H for binding of various ligands to the human sweet receptor T1R2/T1R3

T1R2/T1R3	**RebC**	**Rubusoside**	**RebM**	**RebD**
TMD2 open (No C20)	0.276	0.363	0.303	
TMD3 open (No C20)	0.506	0.199	0.549	0.219
TMD2 open (+C20)	1.000		0.748	
TMD3 open (+C20)	0.115	0.927	0.246	0.843

For instances where the Hill slope n_H is less than 1, suggesting negative cooperativity, the binding site number (N) satisfies the condition $N \geq \frac{1}{n_H}$.[117] Table 2 might contain errors in the Hill slope due to the errors inherent in experimental measurements and the curve fitting process. When the Hill slope n_H is significantly less than 1, it is considered indicative of multiple binding sites. In Table 2, all four sweet ligands, RebC, Rubu, RebD, and RebM, exhibit instances where the Hill slope is significantly less than 1. Following the experimental principle $N \geq \frac{1}{n_H}$, this suggests that these four sweet ligands possess multiple binding sites on the human T1R2/T1R3 sweet receptor.

Considering the sweetness levels of the ligands in Table 1, RebC is categorized as a low-sweet ligand, while RebM and RebD are categorized as high-sweet ligands, with RebM slightly surpassing RebD in sweetness. Rubu falls in the intermediate sweetness category, positioned between RebD and the low-sweet RebC. In Table 1, across all scenarios involving human sweet T1R2/T1R3 receptors, the binding constant K_d consistently shows an inverse correlation with sweetness, except for RebD. Despite having similar sweetness to RebM, RebD deviates from this pattern, suggesting lower efficiency in transmitting the sweetness biological signal. The stronger binding affinity of RebD results in a lower sweetness signal compared to RebM. In all cases where G protein C20 is introduced to the microtoroid functionalized with sweet T1R2/T1R3 receptors before sweet ligand injection, a significant reduction in the binding constant k_d is observed. This

implies that the coupling of G protein C20 to the TMD of the T1R2/T1R3 heterodimer enhances the heterodimer sweet receptor's binding affinity upon its first activation.

The interaction with antibodies elicits distinct effects on the T1R2/T1R3 sweet receptor. Attaching antibodies to the Helix 8 C-terminus of the GPCR places them at a significant distance from the extracellular TMD binding site, indicating minimal impact on sweet ligand binding at the TMD binding site. When the antibody is attached to the TMD Helix 8 site, potentially involved in G protein coupling to TMD, it may impede C20 binding to TMD. In the absence of C20, RebM and RebC exhibit a lower binding constant K_d in the TMD2 open case than the TMD3 open case. According to the Hill slope n_H for the multiple binding of negative cooperativity binding in the supplementary information, the enhanced binding affinity at the orthosteric binding site leads to a decrease in the binding constant K_d with an increase in Hill slope n_H. The elevated Hill slope in the TMD2 open case suggests increased binding affinity at the orthosteric binding site (VFD2), as indicated by docking simulations for RebM and RebC. The anti-flag antibody coupled to TMD2 may reorient TMD2 to stabilize the VFD2 conformation through CRD2, enhancing VFD2 binding affinity for RebM and RebC. Notably, this antibody's enhancement effect is relatively weaker compared to that of G protein C20 coupling to TMD. However, for Rubu, whose orthosteric binding site is VDF3 as indicated by docking simulations, the binding constant K_d remains largely unchanged between the TMD2 open case and TMD3 open case in the absence of C20. The TMD3 open case's Hill slope even shows a slight decrease, suggesting that the anti-rho antibody coupled to TMD3 may not enhance the VFD3 binding affinity for Rubu. It appears that the anti-rho antibody coupled to TMD3 does not induce reorientation of TMD3 or stabilize the VFD3 conformation but don't enhance the VFD3 binding affinity for Rubu.

In the presence of G protein C20, RebM and RebC exhibit a lower binding constant $K_d$transitioning from the TMD3 open case to the TMD2 open case, especially for the high-sweet RebM. Simultaneously, the Hill slope of the TMD2 open case is higher than the TMD3 open case, indicating enhanced binding affinity at the orthosteric binding site (VFD2). For RebM and RebC in the TMD3 open case, the presence of C20 results in a lower binding constant K_d and Hill slope n_H compared to the absence of C20. As per the Hill slope n_H for the multiple binding case for the negative cooperativity binding in the supplementary information, the orthostatic binding site's binding affinity enhancement, causes the binding constant K_d to decrease with a decrease in Hill slope n_H. Therefore, G protein coupling to TMD3 enhances the orthostatic binding site of RebM and RebC, which could be VFD3, TMD2, or TMD3. For Rubu, whose orthosteric binding site is VFD3, in the TMD3 open case, the binding constant $K_d$decreases with C20 coupling to TMD3. Simultaneously, the presence of G protein C20 increases the Hill slope n_H close to 1, signifying enhancement at the orthosteric binding site VFD3. The experimental results suggest that G protein might bind to both TMD3 and TMD2 intracellular regions and enhance the binding of the corresponding binding sites VFD2 and VFD3 separately for the Steviol Rebaudiosides.

In silico binding energies

Docking results of various Rebs at multiple binding sites, VFD2, VFD3, TMD2, and TMD3:

All docking results of various steviol glycosides with or without C20 at VFD2, VFD3, TMD2, and TMD3 are summarized in Table 3. Based on UCavE, most of steviol glycosides without C20 prefers to bind at the orthosteric binding site, cVFD2, except RebB and Rubu.

Compared to the orthosteric binding site (UCav E: -64.66 kcal/mol), Rubu which is the smallest steviol glycoside shows more stable interaction at VFD3 (UCav E: -82.41 kcal/mol), where natural sugars, sucrose or fructose, can also bind.

RebB is the only ligand with a charged group among the steviol glycosides, which was used as a radiolabeled ligand for this binding study. Because of the presence of the charged group, RebB showed a different binding preference compared to other steviol glycosides. It has much favorable interactions at TMDs (UCav E: -98.53 kcal/mol for TMD3, -96.11 kcal/mol for TMD2) rather than VFD2 (UCav E: -72.84 kcal/mol). As shown in Fig. 2, the carboxylate group at the R1 site of RebB can form a salt bridge with R725 (5.37) at TMD2 and with the protonated H734 (5.44) at TMD3. RebB also has several H-bonds at the backbone of L719 (EC2) /S726 (EC2) and the side chains of R790 (7.34) at TMD3. The best binding site for RebB is the allosteric binding site, TMD3. Thus, this preferred binding of RebB at TMD3 and not VFD2 results in ambiguous data for RebM at VFD2 from the radio-labeled ligand binding study in Table 3.

When C20 is present at TMD3, all four cases of RebM, RebD, RebC, and Rubu prefer to bind to the orthosteric binding site, VFD2. However, when C20 is present at TMD2, RebM and RebD with high sweetness do not affect the binding preference, while Rubu and RebC with low sweetness differs in the binding preference (Table 3). The order of UCav binding energy differs in the low sweet cases. Rubu first binds at oVFD3, while RebC first binds at TMD3.

Table 3. Sweetness data at 300 ppm[20] and calculated binding energies (kcals/mol) of various steviol glycosides at closed venus fly trap domain 2 (cVFD2), transmembrane domain 2 (TMD2), TMD3 and open VFD3. The binding energy (BE) was ordered unified cavity energy (UCav E), which is the sum of the non-bonding energy in the unified binding site within 5 Å of ligands.

Ligand	Sweetness at 300ppm	Ucav E (kal/mol)				BE order
		cVFD2	TMD2	TMD3	oVFD3	
Reb1-5	7.40	-156.96	-102.72	-26.20	-38.83	VFD2>TMD2>VFD3>TMD3
RebM	6.55	-135.74	-89.80	-34.23	-7.09	VFD2>TMD2>TMD3>VFD3
RebD	6.15	-123.85	-70.85	-47.90	-86.27	VFD2>VFD3>TMD2>TMD3
isoRebM	6.01	-119.92	-79.40	-40.36	-48.98	VFD2>TMD2>VFD3>TMD3
RebA	5.90	-104.15	-70.92	-85.19	-82.31	VFD2>TMD3>VFD3>TMD2
RebB	5.20	-72.84	-96.11	-98.53	-24.48	TMD3>TMD2>VFD2>VFD3
Rubu	3.87	-64.66	-52.21	-61.30	-82.41	VFD3>VFD2>TMD3>TMD2
Reb1-2	3.13	-178.39	-102.69	-57.41	-38.29	VFD2>TMD2>TMD3>VFD3
RebC	2.64	-101.22	-97.15	-77.10	-52.18	VFD2>TMD2>TMD3>VFD3
hydRebM	1.14	-125.02	-91.55	-42.71	-44.69	VFD2>TMD2>VFD3>TMD3
Ligand	C20 at TMD3	Ucav E (kal/mol)				BE order
		VFD2	TMD2	TMD3	oVFD3	
RebM		-125.44	-86.23	-17.96	-102.80	VFD2>VFD3>TMD2>TMD3

RebD		-98.10	-80.84	-74.23	-70.02	VFD2>TMD2>TMD3>VFD3
Rubu		-84.77	-61.66	-39.08	-42.10	VFD2>TMD2>VFD3>TMD3
RebC		-94.57	-79.47	-75.47	-40.81	VFD2>TMD2>TMD3>VFD3
Ligand	C20 at TMD2	Ucav E (kal/mol)				BE order
		VFD2	TMD2	TMD3	oVFD3	
RebM		-98.37	-52.10	-64.81	-95.54	VFD2>VFD3>TMD3>TMD2
RebD		-85.13	-75.83	-60.62	-82.11	VFD2>VFD3>TMD2>TMD3
Rubu		-43.88	-69.10	-50.80	-75.95	VFD3>TMD2>TMD3>VFD2
RebC		-79.54	-43.27	-83.24	-71.82	TMD3>VFD2>VFD3>TMD2

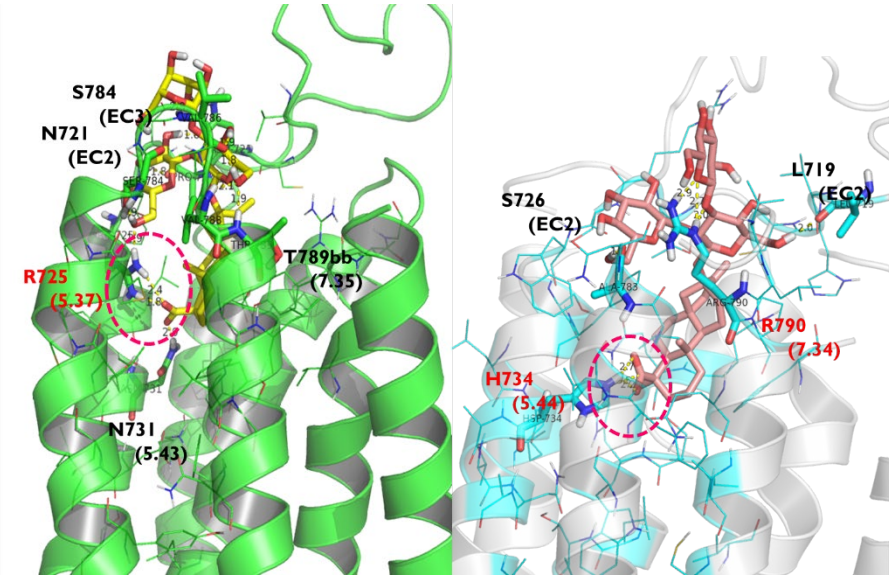

Figure 2. The binding poses of RebB at T1R2 TMD (Left) and T1R3 TMD (Right). The salt bridge is displayed in the dotted circle. The carboxylate group at R1 site of RebB can form the salt bridge with R725 (5.37) at TMD2 and the protonated H734 (5.44) at TMD3, respectively.

Docking result of various ligands

T1R2/T1R3 TMD3 binders: Cyclamate allosteric agonist, Neohesperidin dihydrochalcone (NHDC) artificial sweetener, and lactisole negative allosteric modulator are well-known TMD3 binders to the T1R2/T1R3 heterodimer. When we used lactosole as a radio-labeled ligand, the VFD2 binder Ace-K (artificial sweetener) and the TMD2 binder S819 (positive allosteric modulator) do not compete with lactisole (Table 4). However, TMD3 binder NHDC shows the highest inhibition with Ki of 333.7 µM among the 6 ligands (RebM, RebC, Ace-K, S819, NHDC, and amiloride). Our docking study also found that NHDC has the lowest UCav binding E (the second lowest BE), consistent with the highest inhibition (K_i) among six ligands (Table 4). From the experimental observation, the NHDC binding site at the human sweet taste receptor overlaps with those for the sweetener cyclamate and the sweet taste inhibitor lactisole.[81] The observed

binding site of cyclamate and/or lactisole are Q636 (3.28), Q637 (3.29), S640 (3.32), H641 (3.33), H721 (EC2), R723 (5.36), S729 (5.42), F730 (5.43), A733 (5.46), F778 (6.51), V779 (6.52), L782 (6.55), R790 (7.34), and L798 (7.36) of hT1R3. Additional important amino acids for NHDC binding are Y699 (4.60), W775 (6.48), and C801 (7.39) from point-mutation experiments. From our docking study, NHDC forms multiple H-bonds at the backbone of F624 (2.60) and V720 (EC2) and with the side chains of Q636 (3.28), Q637 (3.29), S640 (3.32), C722 (EC2), S726 (EC2), R790 (7.34), and Q794 (7.38), as shown in Fig. 3.

Steviol glycosides, RebC and RebM, also show mM level binding affinities, 6.98 and 11.75, respectively. RebC has better scoring energies than RebM does, which also agrees with experimental observations.

Ligands that bind to other sites, Ace-K, S-819, and amiloride, reveal higher binding energy at TMD3, which also have fewer H-bonds. As shown in Fig. 3, S819 has H-bonds at H641 (3.33) and N737 (5.47). Amiloride forms H-bonds at S640 (3.32), C722 (EC2), R723 (EC2), R790 (7.34), and Q794 (7.38). Ace-K has H-bonds at Q637 (3.29) and R790 (7.34).

Table 4. The binding affinity (Ki, M) for TMD3 binding using the radio labelled ligand, lactisole and the scoring energy (UCav, BE, SolvE) from the docking study. Lactisole was used as a radio-labeled ligand. The ligands were ordered by UCav E. The agreement with the experiment is shown in bold, while the disagreement with the experiment is displayed in italic.

Ligand	**Ki (mM)**	**UCav**	**BE**	**SolvE**
RebB	N.A.	-98.96	-134.05	-22.17
NHDC	0.33	**-89.28**	**-124.72**	**-86.05**
RebA	N.A.	-84.67	-141.65	-58.73
RebC	6.98	**-76.44**	*-126.12*	**-60.65**
Rubu	N.A.	-60.22	-104.68	-52.59
S819	N.C.	-50.89	-59.95	-40.16
Amiloride	-	-34.26	-58.34	-39.84
RebM	11.75	**-33.13**	**-121.89**	**-35.84**
AceK	N.C.	-29.68	-38.23	-31.38

- N.A.: not available, N.C.: not compete

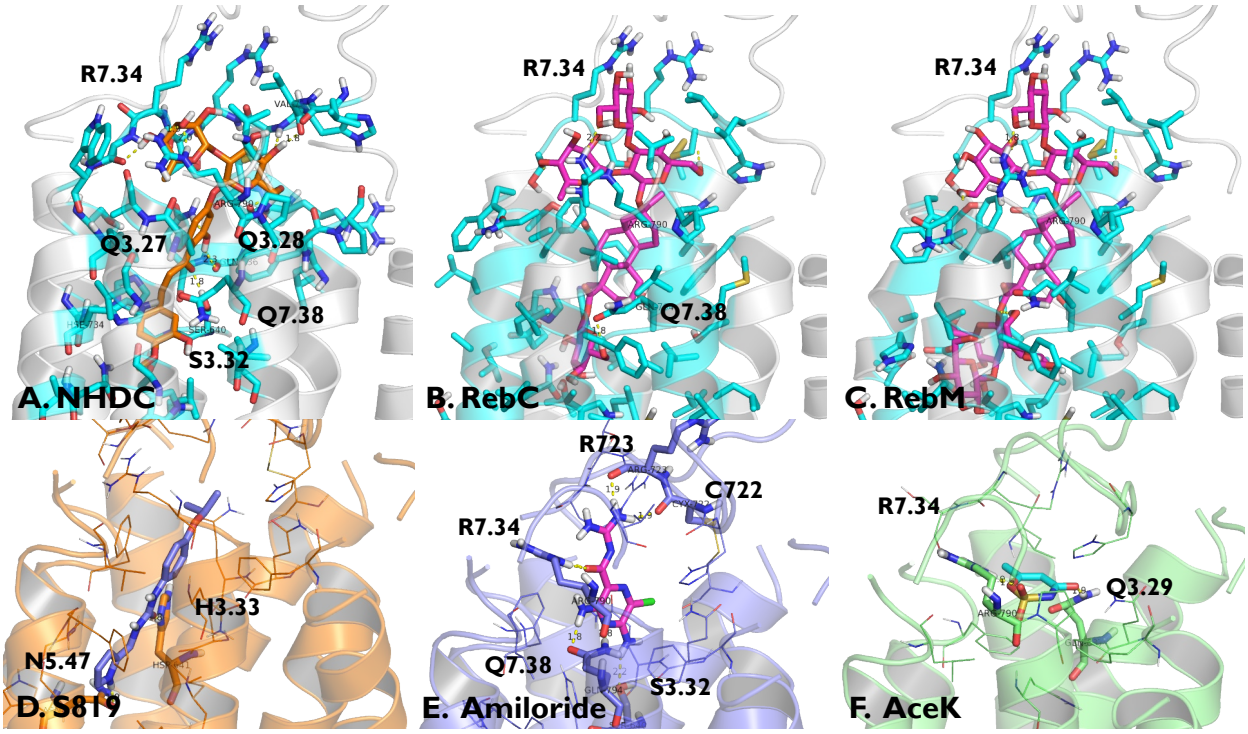

Figure 3. The binding poses of A) NHDC, B) RebC, C) RebM, D) S819, E) Amiloride, and F) Ace-K at TMD3 of T1R2/T1R3 heterodimer.

T1R2/T1R3 VFD2 binders: Artificial sweeteners saccharin and aspartame as well as natural sweeteners sugar and stevioside can bind to VFD2 of T1R2/T1R3 heterodimer. From the docking study, we found RebM, which has high sweetness, shows the lowest binding E in all scoring energies (UCav, BE, SolvE), although RebM gave an ambiguous result in experiment because of its low solubility (Table 5). The second lowest E is from RebC, which has lower sweetness than does RebM. Ace-K has the highest K_d values (bad binder to VFD2), resulting in the highest binding energy. However, the best binder to VFD2 was amiloride (TMD2 binder), although the binding energy shows it to be unfavorable. In addition, several ligands known to bind TMD2 or TMD3 were found at the detected level of the binding affinity. The third lowest one by UCav and BE is the TMD3 binder NHDC, which displays a slightly lower binding affinity. One possibility of these mixed data is the multiple binding sites of RebB used for the radiolabeling. Based on the experiment (Table 4), since RebC can bind to TMD3, RebB without sugars at the R1 position which is smaller than RebC is also predicted to bind to TMD3. As shown in Fig. 4, S819 and Ace-K have two H-bonds at D142 and R383. Amiloride forms multiple H-bonds at Y103, N143, S165,D278, and R383. NHDC has H-bonds at N44, N143, D213, and R383. RebM made H-bonds at S40, D142, D278, D307, R339, and R383. Our docking pose of RebB at the binding site of TMD3 shows the possibility of a salt-bridge at the protonated histidine, H734 (5. 44), as shown in Fig. 2 (Right). Based on our docking study, RebB can also bind to TMD2. Supporting this, RebB at the binding site of TMD2 formed a salt-bridge at R725 (5.37) as well as H-bonds at N731 (5. 43) with the terminal carboxylate (Fig. 2 left). So, the high binding affinity data of amiloride might arise from TMD2 binding. The other possibility derives from the multiple binding sites of the tested ligands. For example, amiloride (TMD2 binder) could bind to multiple binding sites because

of its small size and its ability to form multiple H-bonds. Thus, this discrepancy arises from mixed data of multiple binding sites of tested ligands as well as the radio labelled ligand.

Table 5. The binding inhibition constants (Ki, M) for VFD2 binding using the radio labelled ligand, RebB and the scoring energy (UCav, BE, SolvE) from the docking study. The ligands are ordered by UCav E. The agreement with the experiment is shown in bold, while the disagreement with the experiment is displayed in italic.

Ligand	Ki (mM)	UCav	BE	SolvE
RebM	*Ambiguous*	-132.58	-209.99	-174.32
RebA	N.A.	-104.33	-149.66	-120.72
RebC	18.99	**-98.94**	**-141.82**	**-105.55**
NHDC	*63.37*	**-75.28**	**-122.49**	**-90.06**
RebB	N.A.	-69.61	-125.98	-101.37
S819	Ambiguous	-49.86	-76.06	-47.80
Amiloride	*1.35*	**-29.34**	**-56.26**	**-51.41**
AceK	1096.00	**-25.09**	**-35.34**	**-28.07**

- N.A.: not available

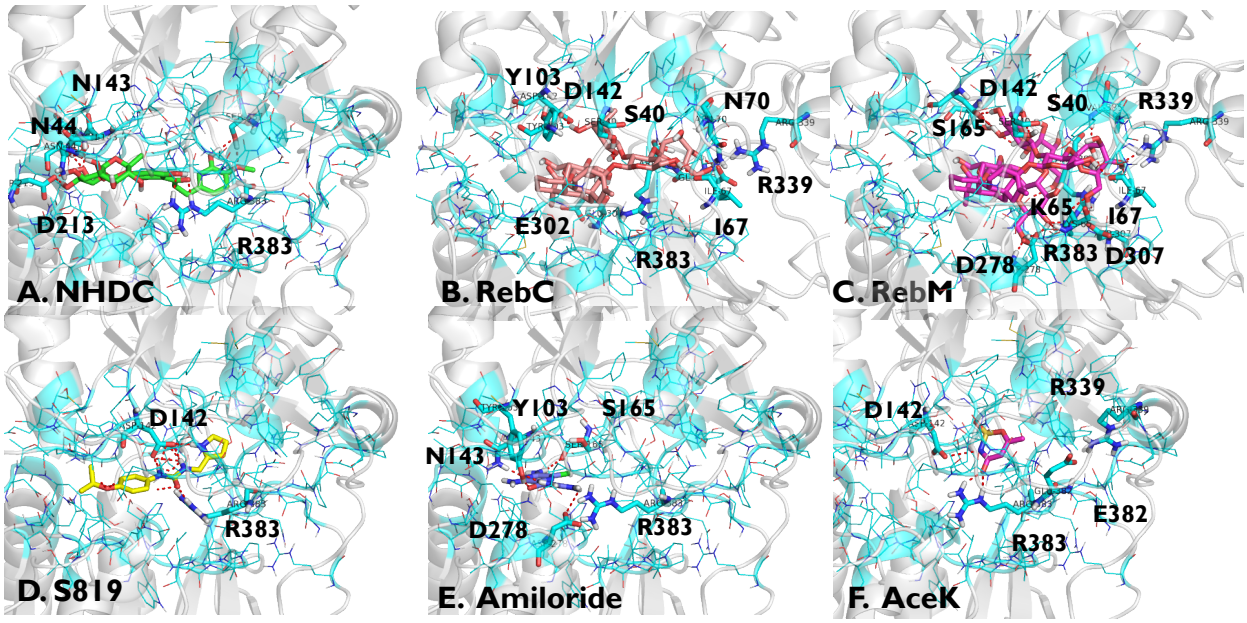

Figure 4. The binding poses of A) NHDC, B) RebC, C) RebM, D) S819, E) Amiloride, and F) Ace-K at TMD3 of T1R2/T1R3 heterodimer.

T1R2/T1R3 TMD2 binders: Allosteric agonist perillatine, antagonist amiloride, and positive allosteric modulator S819 are reported as the TMD2 binders of T1R2/T1R3 heterodimer. From the experiment for testing the binding affinity at TMD2 (Table 6) using perillartine for radiolabeling, there are many ambiguous data. Even TMD2 binders such as S819 and amiloride result in

ambiguities. Unexpectedly, Ace-K (VFD2 binder) and NHDC (TMD3 binder) reveal a detected level of the binding affinity.

From the docking study, we have good agreement for three cases (S819, NHDC, amiloride). NHDC has a better binding energy than does S-819 or amiloride. However, Ace-K is less favorable than NHDC. Since perillartine (agonist) has a structure very similar to amiloride (antagonist), we suspect this mixed data arises from multiple binding sites of the radiolabeled and the test ligand. As shown in Fig. 5, NHDC has the H-bonds at R3.28, S5.51, R5.37, R7.34, and D7.38. RebM made H-bonds at R3.28, K4.53, D5.47, S5.51, and N7.45. S819 has an H-bond at D7.38. Amiloride forms multiple H-bonds at N5.43, T5.44, S6.48 and N7.45. Ace-K has a salt bridge at R5.37 with one H-bond at N5.43.

Table 6. The binding inhibition constants (Ki, mM) for TMD2 binding using the radio labelled ligand, perillartine and the scoring energy (UCav, BE, SolvE) from the docking study. The ligands are ordered by Ucav E. The agreement with the experiment is shown in bold, while the disagreement with the experiment is displayed in italic.

Ligand	**Ki (mM)**	**UCav**	**BE**	**SolvE**
RebB	N.A.	-102.55	-179.98	-27.33
RebC	Ambiguous	-96.95	-143.56	-52.28
NHDC	*293.7*	*-92.24*	*-131.81*	*-83.08*
RebM	Ambiguous	-90.03	-180.89	-96.04
RebA	N.A.	-70.92	-122.32	-56.96
S819	*Ambiguous*	-44.73	-64.23	-47.13
AceK	*142*	*-31.64*	*-37.94*	*-21.55*
Amiloride	*Ambiguous*	*-27.50*	-57.20	-47.35

- N.A.: not available

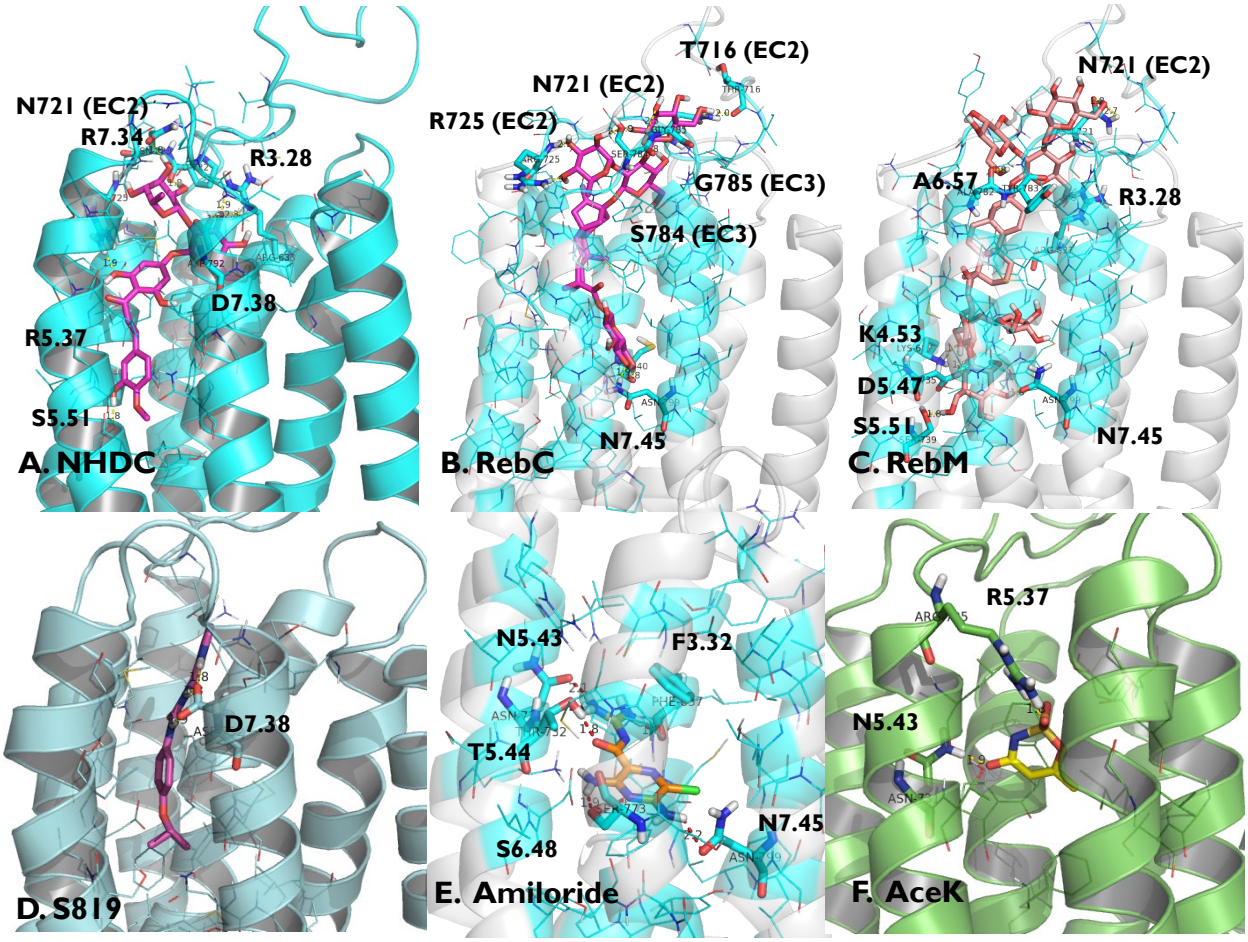

Figure 5. The binding poses of A) NHDC, B) RebC, C) RebM, D) S819, E) Amiloride, and F) Ace-K at TMD2 of T1R2/T1R3 heterodimer.

Docking result of radio-labeled ligands, Perillatin and Lactisole: From the docking study, perillatin, an agonist of the human sweet taste receptor, interacts with N799 (7.37) at TMD2 of T1R2/T1R3 heterodimer with UCav E of -25.92 kcal/mol and BE of -35.28 kcal/mol, as shown in Fig. 6 (Left). Lactisole as a negative allosteric modulator can bind to TMD3 of T1R2/T1R3 heterodimer. From our docking study, lactisole, an inhibitor of the human sweet taste receptor, interacts with S640 (3.32), the protonated H641 (3.33), H734 (5. 44) and Q794 (7.38) at TMD3 of T1R2/T1R3 heterodimer as shown in Fig. 6 (Right). This docking result of lactisole agrees with the inhibitory activity of (±)-lactisole, which was not determined by H641A and Q794N mutation at T1R3 TMD.[28]

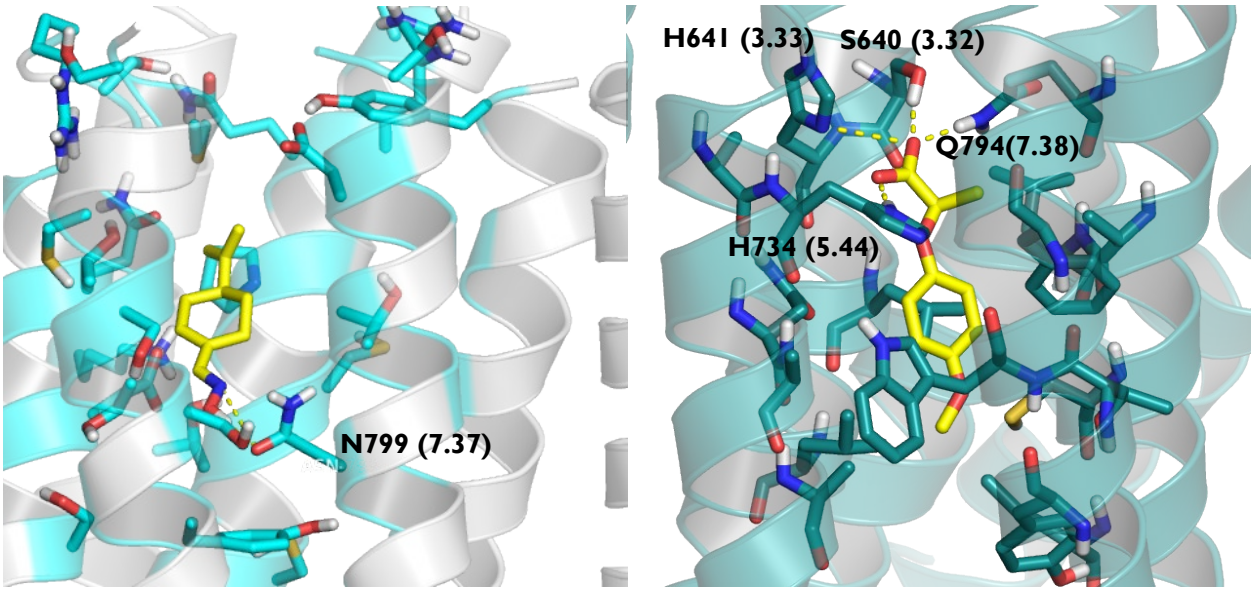

Figure 6. The binding poses of parillatin at TMD2 (Left) and lactosole at TMD3 (Right) of T1R2/T1R3 heterodimer.

In silico binding site discovery

We discovered nine sites using the SiteMap method. The sweet heterodimer appears to have many potential binding sites that make interpretation of the experimental binding data difficult. Two sites discovered correspond to the canonical VFD2 binding site (*in silico* site 5, Figure S15) and VFD3 binding site (*in silico* site 1, Figure S15).

Two additional sites were found near the interaction of the VFD. Site 4 was near the top intersection of the VFD. Site 6 was near the bottom intersection of the VFD. The VFD2 and VFD3 upper distances, near site 4 have been correlated with binding and the active state of the receptor of some ligands.[118] Binding in this site could potentially influence binding and activation. Binding in site 6 could influence the transmission of allosteric movements between the heterodimer section.

Site 9 was found at the intersection of the VFD2 and CRD2. Binding at site 9 could influence the canonical binding site of VFD2.

Two sites (8 and 10) were more associated with TMD, 10 was located at the intersection of TMD2 and CRD2. This was near the sweet protein binding site. Presumably binding at this site could activate the receptor. Finally, site 8 is located on the intracellular side of TMD3. Binding at this site could potentially impact the G protein if it is bound on TMD3.

The δG of binding from MM/GBSA (Table S4) are shown below for high sweet (RebB) medium sweet (Rubu) and low sweet (RebC) ligands. Site 5 in Fig. S15 was selected as the canonical VFD2 binding site and MM/GBSA values are shown as the delta from those of site 5 to enable a comparison. Sites 2, 6 and 10 show better relative binding than site 5 (VFD2) from RebB. RebC showed the same but with the addition of site 8. Rubu showed less favorable relative binding at all sites probably due to the smaller size and less sugar attachments.

The SiteMap analysis indicates the potential for several non-canonical binding sites that could influence the interpretation of experimental binding results.

CONCLUSIONS

In conclusion, we carried out a comprehensive investigation into multiple binding sites for Steviol Rebaudiosides at the human sweet taste heterodimer, integrating experimental results with computational simulations. The cell-free stable heterodimer used in FLOWER enabled a direct measurement of the Steviol Rebaudiosides ligand binding response, leading to determination of the binding constant (K_d). In comparison to the previously reported EC_{50} value for RebM (29.54μM) using cell-based methods, our K_d value for RebM was notably lower, possibly from the use of a cell-free method that directly measured binding responses from the T1R2/T1R3 heterodimer, avoiding downstream signaling variability in cells.

Our docking results support multiple binding sites of the tested ligands as well as the radio labelled ligand, which can explain the mixed data of the radio-ligand binding experiments. We found different preferred binding sites depending on the ligand modification of steviol glycosides; Rubu binds at VFD3, while RebB binds at TMD3. The radioligand depletion experiment on competitive binding provided valuable insights into the binding sites for RebC and RebM. Specifically, RebM and RebC exhibited competitive binding on TMD3, while they did not share binding pockets with perillartine on TMD2. Additionally, RebC and RebM displayed binding on VFD2, with RebC sharing binding pockets with RebB on VFD2, while RebM did not bind to RebB's binding pockets on VFD2. Despite the comprehensive nature of our modeling simulations, some discrepancies emerged that challenge the alignment with experimental data. A potential explanation may lie in the omission of antibody coupling to the TMD C-terminal in our model. Molecular docking, however, successfully predicted the preferred binding sites for RebC, Rubu, RebM, and RebD, serving as fundamental information for the preferred binding of Steviol Rebaudiosides.

Analysis of the FLOWER experiment results revealed significant insights into the interaction between the sweet taste receptor T1R2/T1R3 and Steviol Rebaudiosides. In the FLOWER experiment, we observed that G protein coupling may occur at both TMD2 and TMD3. This coupling event had distinct effects on ligand binding affinity, with G protein coupling to TMD3 enhancing Rubu binding affinity at the VFD3 binding site. For RebC and RebM, G protein coupling to TMD2 enhanced VFD2 binding, while G protein coupling to TMD3 increased the binding affinity for VFD3 and TMD3. In the absence of G protein coupling during the FLOWER binding experiment, the sweet heterodimer exhibited the presence of multiple binding sites, a finding substantiated by the discovery of nine binding sites in the human sweet taste receptor through SiteMap simulations. Thus, we observed GPCR allostery using the label free FLOWER method; C20 G protein binding can alter GPCR affinity to the high-affinity state for steviol glycosides. This observation lends support to the hypothesis that the activation process of the sweet heterodimer is intricately modulated by G protein coupling. Without the G protein, the activation of the sweet ligand-binding may fail to sufficiently stabilize the heterodimer conformation, potentially leading to the opening of numerous binding pockets for Steviol Rebaudiosides ligands.

The identification of multiple binding sites on the T1R2/T1R3 heterodimer for Steviol Rebaudiosides ligands emphasizes the inherent complexity in ligand-receptor interactions. This discovery establishes a solid foundation for continued exploration within the realms of sensory perception and molecular studies. These studies increase a better understanding of the structure of this heterodimeric sweet taste receptor and can act as a guide for rational structure-based design of novel non-caloric sweeteners, which can be used in a novel therapeutic application for treatment

of obesity and related metabolic dysfunctions such as diabetes as well as a novel sweet enhancer that can enable lower sugar usage levels while retaining the sweet taste.

ACKNOWLEDGMENTS

Funding for this project was provided by a grant from Cargill Global Food Research and NIH (R01HL155532 to WAG and R35GM137988 to JS). S. Robles, as an undergraduate research assistant, participated in surface functionalization of the microtoroid resonators in the initial experimental stages.

Conflict of interest

J.S. owns a financial stake in Femtorays Technologies which develops label-free molecular sensors.

Supporting Information Available:

Table S1. Competition binding experiments of various ligands with [^{3}H]-Rebaudioside B, Table S2. Competition binding experiments using [^{3}H]-Lactisole as radioligand against Ligand, Table S3. Competition binding experiments using [^{3}H]-Perillartine as radioligand, Table S4. The free energy of the binding of steviol glycosides to heterodimeric sweet taste receptor (T1R2/T1R3) using Molecular mechanics with generalized Born and surface area solvation (MM/GBSA), Figure S1. Overview of Frequency Locked Optical Whispering Resonator (FLOWER) System, Figure S2. FLOWER binding response to increasing concentrations of sweet ligand onto human sweet receptors T1R2/T1R3, Figure S3. Normalized binding response curve of various sweet ligands binding to the human sweet receptor T1R2/T1R3 for various conditions, Figure S4. Kinetic binding using [^{3}H]-Rebaudioside B as radioligand, Figure S5. Effect of GDP on the binding of [^{3}H]-Rebaudioside B, Figure S6. Effect of GTP on the binding of [^{3}H]-Rebaudioside B, Figure S7. Kinetic binding using [^{3}H]-Lactisole as radioligand, Figure S8. Effect of GDP on the binding of [^{3}H]-Lactisole, Figure S9. Effect of GTP on the binding of [^{3}H]-Lactisole, Figure S10. Kinetic binding using [^{3}H]-Perillartine as radioligand, Figure S11. Effect of GDP on the binding of [^{3}H]-Perillartine, Figure S12. Effect of GTP on the binding of [^{3}H]-Perillartine, Figure S13. Kinetic binding using [^{14}C]-sucrose as radioligand, Figure S24. Competition binding curve of variable concentration of NHDC against fixed concentration of [^{14}C]-sucrose, Figure S15. All putative binding sites of steviol glycosides obtained through SiteMap study.

References

1. Nie, Y., Vigues, S., Hobbs, J. R., Conn, G. L. & Munger, S. D. Distinct Contributions of T1R2 and T1R3 Taste Receptor Subunits to the Detection of Sweet Stimuli. *Current Biology* **15**, 1948–1952 (2005).
2. DuBois, G. E. Molecular mechanism of sweetness sensation. *Physiology & Behavior* **164**, 453–463 (2016).
3. Lindemann, B. Taste reception. *Physiological Reviews* **76**, 719–766 (1996).
4. Chandrashekar, J., Hoon, M. A., Ryba, N. J. P. & Zuker, C. S. The receptors and cells for mammalian taste. *Nature* **444**, 288–294 (2006).

5. Lustig, R. H., Schmidt, L. A. & Brindis, C. D. The toxic truth about sugar. *Nature* **482**, 27–29 (2012).

6. Kuhn, C. *et al.* Bitter Taste Receptors for Saccharin and Acesulfame K. *J. Neurosci.* **24**, 10260–10265 (2004).

7. Max, M. *et al.* Tas1r3, encoding a new candidate taste receptor, is allelic to the sweet responsiveness locus Sac. *Nat Genet* **28**, 58–63 (2001).

8. Sainz, E., Korley, J. N., Battey, J. F. & Sullivan, S. L. Identification of a novel member of the T1R family of putative taste receptors. *Journal of Neurochemistry* **77**, 896–903 (2001).

9. Pin, J.-P. *et al.* The activation mechanism of class-C G-protein coupled receptors. *Biol Cell* **96**, 335–342 (2004).

10. Pin, J.-P., Galvez, T. & Prézeau, L. Evolution, structure, and activation mechanism of family 3/C G-protein-coupled receptors. *Pharmacology & Therapeutics* **98**, 325–354 (2003).

11. Li, X. *et al.* Human receptors for sweet and umami taste. *Proceedings of the National Academy of Sciences* **99**, 4692–4696 (2002).

12. Assadi-Porter, F. M., Tonelli, M., Maillet, E. L., Markley, J. L. & Max, M. Interactions between the human sweet-sensing T1R2–T1R3 receptor and sweeteners detected by saturation transfer difference NMR spectroscopy. *Biochimica et Biophysica Acta (BBA) - Biomembranes* **1798**, 82–86 (2010).

13. Maillet, E. L. *et al.* Characterization of the Binding Site of Aspartame in the Human Sweet Taste Receptor. *Chemical Senses* **40**, 577–586 (2015).

14. Masuda, K. *et al.* Characterization of the Modes of Binding between Human Sweet Taste Receptor and Low-Molecular-Weight Sweet Compounds. *PLOS ONE* **7**, e35380 (2012).

15. Nuemket, N. *et al.* Structural basis for perception of diverse chemical substances by T1r taste receptors. *Nature Communications* **8**, 15530 (2017).

16. Xu, H. *et al.* Different functional roles of T1R subunits in the heteromeric taste receptors. *Proceedings of the National Academy of Sciences* **101**, 14258–14263 (2004).

17. Zhang, F. *et al.* Molecular mechanism of the sweet taste enhancers. *Proceedings of the National Academy of Sciences* **107**, 4752–4757 (2010).

18. Pierce, K. L., Premont, R. T. & Lefkowitz, R. J. Seven-transmembrane receptors. *Nature Reviews Molecular Cell Biology* **3**, 639–650 (2002).

19. Kyriazis, G. A., Soundarapandian, M. M. & Tyrberg, B. Sweet taste receptor signaling in beta cells mediates fructose-induced potentiation of glucose-stimulated insulin secretion. *Proc Natl Acad Sci U S A* **109**, E524–E532 (2012).

20. Kim, S.-K., Chen, Y., Abrol, R., Goddard, W. A. & Guthrie, B. Activation mechanism of the G protein-coupled sweet receptor heterodimer with sweeteners and allosteric agonists. *Proceedings of the National Academy of Sciences* **114**, 2568–2573 (2017).

21. Belloir, C., Brulé, M., Tornier, L., Neiers, F. & Briand, L. Biophysical and functional characterization of the human TAS1R2 sweet taste receptor overexpressed in a HEK293S inducible cell line. *Sci Rep* **11**, 22238 (2021).

22. Li, X. & Servant, G. Functional Characterization of the Human Sweet Taste Receptor: High-Throughput Screening Assay Development and Structural Function Relation. in *Sweetness and Sweeteners* vol. 979 368–385 (American Chemical Society, 2008).

23. Jiang, P. *et al.* The Cysteine-rich Region of T1R3 Determines Responses to Intensely Sweet Proteins *. *Journal of Biological Chemistry* **279**, 45068–45075 (2004).

24. Zhang, F. *et al.* Molecular mechanism for the umami taste synergism. *Proceedings of the National Academy of Sciences* **105**, 20930–20934 (2008).

25. Zhao, M., Xu, X.-Q., Meng, X.-Y. & Liu, B. The Heptahelical Domain of the Sweet Taste Receptor T1R2 Is a New Allosteric Binding Site for the Sweet Taste Modulator Amiloride That Modulates Sweet Taste in a Species-Dependent Manner. *J Mol Neurosci* **66**, 207–213 (2018).

26. Imada, T. *et al.* Amiloride reduces the sweet taste intensity by inhibiting the human sweet taste receptor. *Biochemical and Biophysical Research Communications* **397**, 220–225 (2010).

27. Fujiwara, S. *et al.* Sweeteners interacting with the transmembrane domain of the human sweet-taste receptor induce sweet-taste synergisms in binary mixtures. *Food Chemistry* **130**, 561–568 (2012).

28. Nakagita, T. *et al.* Structural insights into the differences among lactisole derivatives in inhibitory mechanisms against the human sweet taste receptor. *PLOS ONE* **14**, e0213552 (2019).

29. Masuda, T. *et al.* Five amino acid residues in cysteine-rich domain of human T1R3 were involved in the response for sweet-tasting protein, thaumatin. *Biochimie* **95**, 1502–1505 (2013).

30. Cui, M. *et al.* The Heterodimeric Sweet Taste Receptor has Multiple Potential Ligand Binding Sites. *Current Pharmaceutical Design* **12**, 4591–4600 (2006).

31. Sanematsu, K. *et al.* Molecular Mechanisms for Sweet-suppressing Effect of Gymnemic Acids *. *Journal of Biological Chemistry* **289**, 25711–25720 (2014).

32. Servant, G. *et al.* Positive allosteric modulators of the human sweet taste receptor enhance sweet taste. *Proceedings of the National Academy of Sciences* **107**, 4746–4751 (2010).

33. Toda, Y., Okada, S. & Misaka, T. Establishment of a New Cell-Based Assay To Measure the Activity of Sweeteners in Fluorescent Food Extracts. *J. Agric. Food Chem.* **59**, 12131–12138 (2011).

34. Zopun, M. *et al.* Noncaloric Sweeteners Induce Peripheral Serotonin Secretion via the T1R3-Dependent Pathway in Human Gastric Parietal Tumor Cells (HGT-1). *J. Agric. Food Chem.* **66**, 7044–7053 (2018).

35. Murtaza, B. *et al.* Novel GPR120 agonist TUG891 modulates fat taste perception and preference and activates tongue-brain-gut axis in mice. *Journal of Lipid Research* **61**, 133–142 (2020).

36. Ozdener, M. H. *et al.* CD36- and GPR120-Mediated Ca2+ Signaling in Human Taste Bud Cells Mediates Differential Responses to Fatty Acids and Is Altered in Obese Mice. *Gastroenterology* **146**, 995-1005.e5 (2014).

37. Servant, N. B. *et al.* A Dynamic Mass Redistribution Assay for the Human Sweet Taste Receptor Uncovers G-Protein Dependent Biased Ligands. *Frontiers in Pharmacology* **13**, (2022).

38. DuBois, G. E. Validity of early indirect models of taste active sites and advances in new taste technologies enabled by improved models. *Flavour and Fragrance Journal* **26**, 239–253 (2011).

39. DuBois, G. E. *et al.* Concentration—Response Relationships of Sweeteners. in *Sweeteners* vol. 450 261–276 (American Chemical Society, 1991).

40. Hoare, S. R. J. Receptor binding kinetics equations: Derivation using the Laplace transform method. *Journal of Pharmacological and Toxicological Methods* **89**, 26–38 (2018).

41. Witte, W. E. A. de, Danhof, M., Graaf, P. H. van der & Lange, E. C. M. de. In vivo Target Residence Time and Kinetic Selectivity: The Association Rate Constant as Determinant. *Trends in Pharmacological Sciences* **37**, 831–842 (2016).

42. Ennis, D. M. Molecular Mixture Models: Connecting Molecular Events to Perception. in *Chemistry of Taste* vol. 825 32–38 (American Chemical Society, 2002).

43. Bassoli, A. Developing new sweeteners from natural compounds. *Optimising sweet taste in foods* 327–343 (2006).

44. Laffort, P. Analysing and predicting synergy in sweetener blends. *Optimising sweet taste in foods* 349–374 (2006).

45. Vigues, S., Hobbs, J. R., Nie, Y., Conn, G. L. & Munger, S. D. T1R2, T1R3, and the Detection of Sweet Stimuli. in *Sweetness and Sweeteners* vol. 979 65–75 (American Chemical Society, 2008).

46. Assadi-Porter, F. M., Radek, J., Rao, H. & Tonelli, M. Multimodal Ligand Binding Studies of Human and Mouse G-Coupled Taste Receptors to Correlate Their Species-Specific Sweetness Tasting Properties. *Molecules* **23**, 2531 (2018).

47. Choi, Y. *et al.* Correlation between in vitro binding activity of sweeteners to cloned human sweet taste receptor and sensory evaluation. *Food Science and Biotechnology* **30**, 675–682 (2021).

48. Chen, Z.-X., Wu, W., Zhang, W.-B. & Deng, S.-P. Thermodynamics of the interaction of sweeteners and lactisole with fullerenols as an artificial sweet taste receptor model. *Food Chemistry* **128**, 134–144 (2011).

49. Uhlén, S., Schiöth, H. B. & Jahnsen, J. A. A new, simple and robust radioligand binding method used to determine kinetic off-rate constants for unlabeled ligands. Application at α2A- and α2C-adrenoceptors. *European Journal of Pharmacology* **788**, 113–121 (2016).

50. Riddy, D. M. *et al.* Label-Free Kinetics: Exploiting Functional Hemi-Equilibrium to Derive Rate Constants for Muscarinic Receptor Antagonists. *Mol Pharmacol* **88**, 779–790 (2015).

51. Flanagan, C. A. Chapter 10 - GPCR-radioligand binding assays. in *Methods in Cell Biology* (ed. K. Shukla, A.) vol. 132 191–215 (Academic Press, 2016).

52. Su, J. Label-Free Single Exosome Detection Using Frequency-Locked Microtoroid Optical Resonators. *ACS Photonics* **2**, 1241–1245 (2015).

53. Su, J. Label-free Single Molecule Detection Using Microtoroid Optical Resonators. *Journal of Visualized Experiments* (2015) doi:10.3791/53180.

54. Suebka, S., Nguyen, P.-D., Gin, A. & Su, J. How Fast It Can Stick: Visualizing Flow Delivery to Microtoroid Biosensors. *ACS Sens.* **6**, 2700–2708 (2021).

55. Hao, S. & Su, J. Noise-Induced Limits of Detection in Frequency Locked Optical Microcavities. *Journal of Lightwave Technology* **38**, 6393–6401 (2020).

56. Li, C., Teimourpour, M. H., McLeod, E. & Su, J. Enhanced whispering gallery mode sensors. in *Chemical, Biological, Radiological, Nuclear, and Explosives (CBRNE) Sensing XIX* vol. 10629 79–85 (SPIE, 2018).

57. Su, J. Label-Free Biological and Chemical Sensing Using Whispering Gallery Mode Optical Resonators: Past, Present, and Future. *Sensors* **17**, 540 (2017).

58. Abrol, R., Bray, J. K. & Goddard III, W. A. Bihelix: Towards de novo structure prediction of an ensemble of G-protein coupled receptor conformations. *Proteins: Structure, Function, and Bioinformatics* **80**, 505–518 (2012).

59. Bray, J. K., Abrol, R., Goddard, W. A., Trzaskowski, B. & Scott, C. E. SuperBiHelix method for predicting the pleiotropic ensemble of G-protein–coupled receptor conformations. *Proceedings of the National Academy of Sciences* **111**, E72–E78 (2014).

60. Griffith, A. R. DarwinDock and GAG-Dock: Methods and applications for small molecule docking. (2017).

61. Yang, M. Y., Mafi, A., Kim, S.-K., Goddard, W. A. & Guthrie, B. Predicted structure of fully activated human bitter taste receptor TAS2R4 complexed with G protein and agonists. *QRB Discovery* **2**, e3 (2021).

62. Yang, M. Y., Kim, S.-K., Kim, D., Liggett, S. B. & Goddard III, W. A. Structures and agonist binding sites of bitter taste receptor TAS2R5 complexed with Gi protein and validated against experiment. *The Journal of Physical Chemistry Letters* **12**, 9293–9300 (2021).

63. Tokmakova, A. *et al.* Predicted structure and cell signaling of TAS2R14 reveal receptor hyper-flexibility for detecting diverse bitter tastes. *Iscience* **26**, 106422 (2023).

64. Abrol, R. *et al.* Ligand- and mutation-induced conformational selection in the CCR5 chemokine G protein-coupled receptor. *Proceedings of the National Academy of Sciences* **111**, 13040–13045 (2014).

65. Mafi, A., Kim, S.-K. & Goddard III, W. A. The dynamics of agonist-β2-adrenergic receptor activation induced by binding of GDP-bound Gs protein. *Nature Chemistry* 1–11 (2023).

66. Mafi, A., Kim, S.-K. & Goddard, W. A. The G protein-first activation mechanism of opioid receptors by Gi protein and agonists. *QRB Discovery* **2**, e9 (2021).

67. Malinska, M., Kim, S.-K., Goddard, W. & Ashok, M. Structural Variation and Odorant Binding for Olfactory Receptors Selected from the Six Major Subclasses of the OR Phylogenetic Tree. *Computational Materials, Chemistry, and Biochemistry: From Bold Initiatives to the Last Mile: In Honor of William A. Goddard's Contributions to Science and Engineering* 855–925 (2021).

68. Mafi, A., Kim, S.-K. & Goddard III, W. A. Mechanism of β-arrestin recruitment by the μ-opioid G protein-coupled receptor. *Proceedings of the National Academy of Sciences* **117**, 16346–16355 (2020).

69. Mafi, A., Kim, S.-K. & Goddard III, W. A. The atomistic level structure for the activated human κ-opioid receptor bound to the full Gi protein and the MP1104 agonist. *Proceedings of the National Academy of Sciences* **117**, 5836–5843 (2020).

70. Shankar, V., Goddard III, W. A., Kim, S.-K., Abrol, R. & Liu, F. The 3D structure of human DP prostaglandin G-protein-coupled receptor bound to Cyclopentanoindole antagonist, predicted using the DuplexBiHelix modification of the GEnSeMBLE method. *Journal of Chemical Theory and Computation* **14**, 1624–1642 (2017).

71. Kim, S.-K., Fristrup, P., Abrol, R. & Goddard III, W. A. Structure-based prediction of subtype selectivity of histamine H3 receptor selective antagonists in clinical trials. *Journal of chemical information and modeling* **51**, 3262–3274 (2011).

72. Kim, S.-K., Riley, L., Abrol, R., Jacobson, K. A. & Goddard III, W. A. Predicted structures of agonist and antagonist bound complexes of adenosine A3 receptor. *Proteins: Structure, Function, and Bioinformatics* **79**, 1878–1897 (2011).

73. Mafi, A., Kim, S.-K. & Goddard III, W. A. The mechanism for ligand activation of the GPCR–G protein complex. *Proceedings of the National Academy of Sciences* **119**, e2110085119 (2022).

74. Yang, M. Y., Kim, S.-K. & Goddard III, W. A. G protein coupling and activation of the metabotropic GABAB heterodimer. *Nature Communications* **13**, 4612 (2022).

75. Li, B. *et al.* Structure and Molecular Mechanism of Signaling for the Glucagon-like Peptide-1 Receptor Bound to Gs Protein and Exendin-P5 Biased Agonist. *Journal of the American Chemical Society* **145**, 20422–20431 (2023).

76. Vo, A.-D. P., Kim, S.-K., Yang, M. Y., Ondrus, A. E. & Goddard III, W. A. Fully activated structure of the sterol-bound Smoothened GPCR-Gi protein complex. *Proceedings of the National Academy of Sciences* **120**, e2300919120 (2023).

77. Liu, B. *et al.* Functional characterization of the heterodimeric sweet taste receptor T1R2 and T1R3 from a New World monkey species (squirrel monkey) and its response to sweet-tasting proteins. *Biochemical and Biophysical Research Communications* **427**, 431–437 (2012).

78. Andersen, G. H., Alexi, N., Sfyra, K., Byrne, D. V. & Kidmose, U. Temporal check-all-that-apply on the sensory profiling of sucrose-replaced sweetener blends of natural and synthetic origin. *Journal of Sensory Studies* **38**, e12838 (2023).

79. Azevedo, B. M., Schmidt, F. L. & Bolini, H. M. A. High-intensity sweeteners in espresso coffee: ideal and equivalent sweetness and time–intensity analysis. *International Journal of Food Science & Technology* **50**, 1374–1381 (2015).

80. Jang, J., Kim, S.-K., Guthrie, B. & Goddard, W. A. I. Synergic Effects in the Activation of the Sweet Receptor GPCR Heterodimer for Various Sweeteners Predicted Using Molecular Metadynamics Simulations. *J. Agric. Food Chem.* **69**, 12250–12261 (2021).

81. Winnig, M., Bufe, B., Kratochwil, N. A., Slack, J. P. & Meyerhof, W. The binding site for neohesperidin dihydrochalcone at the human sweet taste receptor. *BMC Struct Biol* **7**, 66 (2007).

82. Cai, C. *et al.* Characterization of the Sweet Taste Receptor Tas1r2 from an Old World Monkey Species Rhesus Monkey and Species-Dependent Activation of the Monomeric Receptor by an Intense Sweetener Perillartine. *PLOS ONE* **11**, e0160079 (2016).

83. Servant, G., Kenakin, T., Zhang, L., Williams, M. & Servant, N. Chapter Three - The function and allosteric control of the human sweet taste receptor. in *Advances in Pharmacology* (ed. Langmead, C. J.) vol. 88 59–82 (Academic Press, 2020).

84. Jiang, P. *et al.* Identification of the Cyclamate Interaction Site within the Transmembrane Domain of the Human Sweet Taste Receptor Subunit T1R3 * [boxs]. *Journal of Biological Chemistry* **280**, 34296–34305 (2005).

85. Jiang, P. *et al.* Lactisole Interacts with the Transmembrane Domains of Human T1R3 to Inhibit Sweet Taste *. *Journal of Biological Chemistry* **280**, 15238–15246 (2005).

86. Deck, C. M. *et al.* Impact of lactisole on the time-intensity profile of selected sweeteners in dependence of the binding site. *Food Chemistry: X* **15**, 100446 (2022).

87. Sainz, E. *et al.* The G-protein coupling properties of the human sweet and amino acid taste receptors. *Developmental Neurobiology* **67**, 948–959 (2007).

88. Maîtrepierre, E., Sigoillot, M., Pessot, L. L. & Briand, L. Recombinant expression, in vitro refolding, and biophysical characterization of the N-terminal domain of T1R3 taste receptor. *Protein Expression and Purification* **83**, 75–83 (2012).

89. Williams, L. T. & Lefkowitz, R. J. Slowly reversible binding of catecholamine to a nucleotide-sensitive state of the beta-adrenergic receptor. *Journal of Biological Chemistry* **252**, 7207–7213 (1977).

90. Park, J. *et al.* Structural architecture of a dimeric class C GPCR based on co-trafficking of sweet taste receptor subunits. *Journal of Biological Chemistry* **294**, 4759–4774 (2019).

91. Su, J., Goldberg, A. F. & Stoltz, B. M. Label-free detection of single nanoparticles and biological molecules using microtoroid optical resonators. *Light: Science & Applications* **5**, e16001 (2016).

92. Suebka, S., Nguyen, P.-D., Gin, A. & Su, J. How Fast It Can Stick: Visualizing Flow Delivery to Microtoroid Biosensors. *ACS Sens.* **6**, 2700–2708 (2021).

93. Ozgur, E. *et al.* Ultrasensitive Detection of Human Chorionic Gonadotropin Using Frequency Locked Microtoroid Optical Resonators. *Anal. Chem.* **91**, 11872–11878 (2019).

94. Luu, G. T. *et al.* An Integrated Approach to Protein Discovery and Detection From Complex Biofluids. *Molecular & Cellular Proteomics* **22**, (2023).

95. Su, J. Label-Free Single Exosome Detection Using Frequency-Locked Microtoroid Optical Resonators. *ACS Photonics* **2**, 1241–1245 (2015).

96. Lu, T., Su, T.-T. J., Vahala, K. J. & Fraser, S. E. Split frequency sensing methods and systems. (2013).

97. Nguyen, P.-D., Zhang, X. & Su, J. One-Step Controlled Synthesis of Size-Tunable Toroidal Gold Particles for Biochemical Sensing. *ACS Appl. Nano Mater.* **2**, 7839–7847 (2019).

98. Hao, S. & Su, J. Noise-Induced Limits of Detection in Frequency Locked Optical Microcavities. *Journal of Lightwave Technology* **38**, 6393–6401 (2020).

99. Watts, K. S. *et al.* ConfGen: A Conformational Search Method for Efficient Generation of Bioactive Conformers. *J. Chem. Inf. Model.* **50**, 534–546 (2010).

100. Seven, A. B. *et al.* G-protein activation by a metabotropic glutamate receptor. *Nature* **595**, 450–454 (2021).

101. Lin, S. *et al.* Structures of Gi-bound metabotropic glutamate receptors mGlu2 and mGlu4. *Nature* **594**, 583–588 (2021).

102. Shen, C. *et al.* Structural basis of GABAB receptor–Gi protein coupling. *Nature* **594**, 594–598 (2021).

103. Koehl, A. *et al.* Structure of the μ-opioid receptor–Gi protein complex. *Nature* **558**, 547–552 (2018).

104. Mafi, A., Kim, S.-K., Chou, K. C., Güthrie, B. & Goddard, W. A. I. Predicted Structure of Fully Activated Tas1R3/1R3′ Homodimer Bound to G Protein and Natural Sugars: Structural Insights into G Protein Activation by a Class C Sweet Taste Homodimer with Natural Sugars. *J. Am. Chem. Soc.* **143**, 16824–16838 (2021).

105. Bhandarkar, M. *et al.* c 1995-2002 The Board of Trustees of the University of Illinois. All Rights Reserved.

106. Phillips, J. C. *et al.* Scalable molecular dynamics with NAMD. *Journal of Computational Chemistry* **26**, 1781–1802 (2005).

107. MacKerell, A. D. Jr. *et al.* All-Atom Empirical Potential for Molecular Modeling and Dynamics Studies of Proteins. *J. Phys. Chem. B* **102**, 3586–3616 (1998).

108. Feller, S. E., Yin, D., Pastor, R. W. & MacKerell, A. D. Molecular dynamics simulation of unsaturated lipid bilayers at low hydration: parameterization and comparison with diffraction studies. *Biophysical Journal* **73**, 2269–2279 (1997).

109. Halgren, T. New Method for Fast and Accurate Binding-site Identification and Analysis. *Chemical Biology & Drug Design* **69**, 146–148 (2007).

110. Halgren, T. A. *et al.* Glide: A New Approach for Rapid, Accurate Docking and Scoring. 2. Enrichment Factors in Database Screening. *J. Med. Chem.* **47**, 1750–1759 (2004).

111. Friesner, R. A. *et al.* Glide: A New Approach for Rapid, Accurate Docking and Scoring. 1. Method and Assessment of Docking Accuracy. *J. Med. Chem.* **47**, 1739–1749 (2004).

112. Sirin, S. *et al.* A Computational Approach to Enzyme Design: Predicting ω-Aminotransferase Catalytic Activity Using Docking and MM-GBSA Scoring. *J. Chem. Inf. Model.* **54**, 2334–2346 (2014).

113. Lum, C. K. L. & Henkin, R. I. Sugar binding to purified fractions from bovine taste buds and epithelial tissue relationships to bioactivity. *Biochimica et Biophysica Acta (BBA) - General Subjects* **421**, 380–394 (1976).

114. Doornbos, M. L. J. *et al.* Molecular mechanism of positive allosteric modulation of the metabotropic glutamate receptor 2 by JNJ-46281222. *British Journal of Pharmacology* **173**, 588–600 (2016).

115. Servant, N. B. *et al.* A Dynamic Mass Redistribution Assay for the Human Sweet Taste Receptor Uncovers G-Protein Dependent Biased Ligands. *Frontiers in Pharmacology* **13**, (2022).

116. Hulme, E. C. & Trevethick, M. A. Ligand binding assays at equilibrium: validation and interpretation. *Br J Pharmacol* **161**, 1219–1237 (2010).

117. Abeliovich, H. An empirical extremum principle for the hill coefficient in ligand-protein interactions showing negative cooperativity. *Biophysical journal* **89**, 76–79 (2005).

118. Acevedo, W., Ramírez-Sarmiento, C. A. & Agosin, E. Identifying the interactions between natural, non-caloric sweeteners and the human sweet receptor by molecular docking. *Food Chemistry* **264**, 164–171 (2018).